Monitoring for time ordering and time asymmetry of spectral correlations in filtered resonance fluorescence generated from a Λ-type atomic system

Ze-an Peng,[1] Guo-qing Yang,[2] Qing-lin Wu,[1] and Gao-xiang Li[1,*]
[1]*Department of Physics, Huazhong Normal University, Wuhan 430079, China*
[2]*College of Electronics and Information, Hangzhou Dianzi University, Hangzhou 310018, China*

(Received 11 July 2018; revised manuscript received 12 September 2018; published 15 October 2018)

Frequency-resolved correlation (FRC) is investigated in fluorescent emission radiated from a Λ-type atomic system by employing weak coupling regime between quantum emitter and cavities, in which each cavity substituting a Lorentzian filter is assumed to pass through only one fluorescent photon at a time so that the analytical discussions for time orderings can be carried out in a truncated Hilbert space with single-excitation state for each cavity mode. In the limit of bad cavity (large passband width of filter) and short delay, the conditional time ordering amplitudes are introduced with the help of conditioned dressed atom-photon states prepared by preselection to probe into the effect of preferential screening for time orderings of filter-detector systems. Meanwhile, the past quantum state formalism is also applied in FRC to further excavate their collective monitoring effect. Based on the obtained two-mode correlation signals, it is found that, in nonresonant two-photon cascaded processes, bunching and antibunching can appear in two opposite detection orderings, respectively, and can be switched. The physical origin is explored that the two different transition amplitudes of emitted photons from a common spectral band of resonance fluorescence are responsible for opposite time orderings, thus, the imbalance between two complementary time orderings can be enhanced, which is impossible to achieve in resonance fluorescence of two-level atoms. This mechanism is embodied in the conditional time ordering amplitudes produced by this detection theory of cavity modes.

DOI: 10.1103/PhysRevA.98.043828

I. INTRODUCTION

The generation of entangled photon pairs runs through the whole developments of quantum optics [1–4] and quantum communication [5–9]. Being the popular entanglement source, strong correlated photon pairs can be produced from the fluorescent emission via frequency engineering with the help of frequency filtering techniques [10], and can violate the Cauchy-Schwarz inequality and Bell's inequality [11–13]. Meanwhile, the application of frequency resolution in driven quantum emitters opens up a new landscape in photon correlation and statistics [14–18], and indicates that multiphoton successive emission can also display strong high-order correlation, which is attributed to the leapfrog transitions involving virtual states [19,20]. Actually, the cascaded photon source has been chosen to be the valuable ingredient to produce entangled photon pairs in biexciton-exciton cascaded emission of semiconductor quantum dot [21–30], in which strongly correlated paired photons possess definite time orderings embodied by the asymmetry of a second-order correlation signal [31,32]. For a two-level atom, the correlation between two opposite spectral lines is related to the ratio of the two dressed populations [33,34], which seems to be possible to manipulate temporal correlations if two dressed populations are distributed unevenly. Lately, this analogous mechanism is used to actualize the preparation of time orderings via coherent control in a quantum dot modeled by a three-level ladder system, which is forced to emit two photons with preferential time ordering without unitary operating for time orderings [35].

Interference of time orderings has been ulteriorly explored theoretically in Mollow triplet and observed experimentally for the first time in a barium atomic beam [36], which emerges in such situation in which two complementary (opposite) two-photon cascaded emissions are required to initiate from a common state and terminate to a common state that is not necessarily the same as the initial state. In a Mollow triplet, it is well known that the resonance fluorescence from lower and higher sidebands are triggered by two different dressed levels [36–39], interference can not be displayed, but rather is seen between the Rayleigh line and one of the sidebands [36]. However, the second-order correlation of latter is symmetric for alternating detection orderings [33], even if each filter is detuned from the central frequency of its target spectral line [34], because in a two-photon cascaded emission of Rayleigh photon followed by a lower sideband photon, for example, the dressed state transition amplitudes of Rayleigh photon and lower sideband photon are cs and c^2, respectively. In the corresponding opposite two-photon channel, it is still c^2 for sideband photon but $-cs$ for Rayleigh photon, where $c, s = \sqrt{(\bar{\Omega} \pm \Delta)/2\bar{\Omega}}$ with Δ and $\bar{\Omega}$ being the laser detuning from the two-level atomic resonance frequency and general Rabi frequency [36,39]. This implies that photons in each spectral line participate in two opposite time orderings with equal transition rates, thus, the two opposite time orderings always keep balance. In this paper, the dressed Λ-type system is selected as our model to discuss the feasibility of breaking

*gaox@mail.ccnu.edu.cn

this balance to highlight or hide a certain time ordering. As we expect, it is found that the temporal second-order correlation of a pair of photons can be enhanced and suppressed for two opposite detection orderings by tuning driving frequency. This means that the symmetry of time orderings can be broken efficiently in a three-level system and realize which-path information erasure. Compared with previous schemes of time reordering [35,40], we hope that our proposal may provide some elicitations for the manipulation of time orderings to generate polarization entangled photon pairs in semiconductor quantum dot.

Thanks to the spirit of the pioneering sensors method for FRC established by del Valle *et al.* [41], we adopt the weakly coupled regime between quantum emitter and cavities to illustrate the above scheme and reveal the dynamical picture of time orderings, which is obscured by the ultimate filtered correlation signals. Recently, following this method, some new algebraical techniques have also been put forward to address FRC, such as the eigenvalue decomposition method [42] and signal-processing approach [43]. In the spectral filtering process, although photons emitted at different times can be differentiated by the filter, because the passband width of the filter characterizes its average resolution ability that all the detected photons can be treated as such that they possess the same lifetimes specified as the reciprocal of the passband width [44], therefore, each Lorentzian filter can be replaced by a single-mode Fabry-Perot empty cavity activated by the fluorescent photons with frequency of corresponding cavity mode and gives rise to the Lorentzian cavity spectrum without arranging time orderings for original filed operators. On the other hand, we tend to track time orderings after preselection, but its information before two-photon emission is also manifested by the conditional time ordering amplitudes defined in our paper from the conditioned states [45–48], which makes it clear that, in our system, two different transition amplitudes of a common spectral line contribute to two opposite conditional time ordering amplitudes, respectively. Thus, the feasibility of enhancing the asymmetry of time orderings can be discovered analytically by this approach. In addition, we combine the past quantum state formalism [49] with conditioned state to jointly explore how two-photon time orderings are selected by two collective filter-detector monitoring systems.

The outline of this paper is as follows: In Sec. II, the quantum system under our consideration is introduced by reviewing the standard theory of FRC. In Sec. III, in the limit of large filter widths and short delay, conditioned state, and past quantum state are found with the aim of analytically calculating two-mode spectral correlation signals of resonance fluorescence with physically perspicuous forms, making it possible to get insight into the dynamical mechanism of time orderings. Then, in Sec. IV, the features of correlation signals, especially the time symmetry and asymmetry, are discussed in the case of resonant and nonresonant two-photon cascaded processes, respectively, with the comparison of the spectral correlations in Mollow triplet. In addition, the feasibility of converting time orderings and statistical properties of photon pairs by enhancing the asymmetry of two-photon paths with opposite time orderings are also investigated by comparing our results with those in a driven four-level quantum dot. Section V is devoted to supplement the case of narrow filters for completeness, and the results can be understood by the good cavities. Finally, a conclusion is presented in Sec. VI.

II. DESCRIPTION OF QUANTUM SYSTEM

We start our work by reviewing the standard detection theory of FRC, in which the setup mainly consists of a pair of ideal photon detectors with two inserted frequency filters in front of them to extract the fluorescent photons with setting frequencies from quantum emitter, and the correlation signal is read out from the correlator [12,50] or recorded by a streak camera [51]. If the earlier filtered fluorescent photon labeled by a is counted at time t followed by the successive detection for filtered photon b delayed for τ, mathematically, the steady two-photon spectral correlation should be evaluated by the filtered Heisenberg atomic transition operators as [34,52–54]

$$g^{(2)}(a,b,\tau)=\frac{\langle\bar{\sigma}_a^\dagger(t)\bar{\sigma}_b^\dagger(t+\tau)\bar{\sigma}_b(t+\tau)\bar{\sigma}_a(t)\rangle}{\langle(\bar{\sigma}_a^\dagger\bar{\sigma}_a)(t)\rangle\langle(\bar{\sigma}_b^\dagger\bar{\sigma}_b)(t+\tau)\rangle},\tag{1}$$

where the filtered atomic transition operators of quantum emitter accounting for the corresponding resolved fields are related to their original atomic transition operators through the filter response functions as [37,55,56]

$$\bar{\sigma}_i(t)=\int_0^\infty f_i(\tau)\sigma_i(t-\tau)d\tau,\quad(i=a,b).\tag{2}$$

However, what is hidden behind Eq. (1) is the extensive computational complexity involving time-dependent atomic operators with various possible permutations. Until the sensor method was proposed by del Valle *et al.* [41], the mathematical treatment for time orderings was successfully avoided. Here, based on the sensor method, we adopt the detection theory of cavity mode to investigate polychromatic photon correlations of resonance fluorescence in our quantum system, in which each Lorentzian filter is regarded as a single-mode Fabry-Perot empty cavity, thus, our consideration will essentially just be mapping the frequency resolution in resonance fluorescence onto the event that each optical empty cavity is weakly pumped by the fluorescent photons with a small coupling constant between quantum emitter and cavity. Throughout this paper, we are interested in the Lorentzian filters, i.e., $f_i(\tau)=\theta(\tau)\lambda_i e^{-(\lambda_i+i\omega_i)\tau}$ [55,56], where $\theta(\tau)$ is the Heaviside step function for the causality of the filtering event in time domain. The filter half passband width λ_i and setting frequency ω_i correspond to the half of the decay rate $\kappa_i/2$ and frequency of the ith cavity, respectively. With these correspondences at hand, the steady two-mode correlation of spectrally resolved fluorescence fields for arbitrary time delay are expressed by the creation and annihilation operators of corresponding quantized cavity modes

$$\begin{aligned}g^{(2)}(a,b,\tau)&=\frac{\langle a^\dagger(t)b^\dagger(t+\tau)b(t+\tau)a(t)\rangle}{\langle(a^\dagger a)(t)\rangle\langle(b^\dagger b)(t+\tau)\rangle}\\&=\frac{\mathcal{G}^{(2)}(a,b,\tau)}{\mathcal{G}^{(1)}(a)\mathcal{G}^{(1)}(b)},\end{aligned}\tag{3}$$

where the numerator, $\mathcal{G}^{(2)}(a,b,\tau)$, is the unnormalized second-order (cross) correlation function between modes a and b, and $\mathcal{G}^{(1)}(a)$ and $\mathcal{G}^{(1)}(b)$ are the first-order correlation

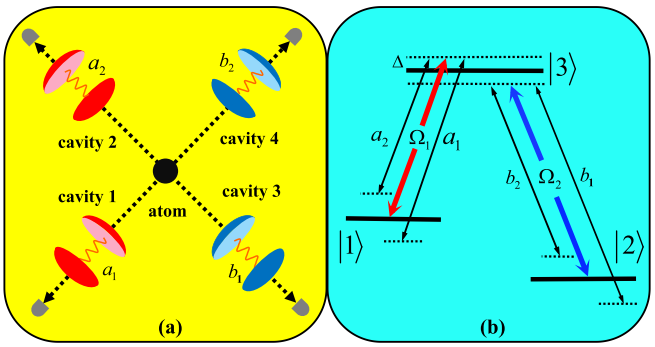

FIG. 1. (a) Equivalent system of atom-photon interactions. Resonance fluorescence is emitted from the excited atom to weakly pump four cavities, and multimode second-order correlations can be realized after four-mode cavity photons are outputted. (b) Level diagram for a Λ-type three-level atom, in which the dipole-allowed transitions $|3\rangle \to |1\rangle$ and $|3\rangle \to |2\rangle$ are driven by two strong applied fields, respectively, and coupled to two-mode quantum fields (a_1, a_2), (b_1, b_2).

functions in modes a and b, respectively, which are essentially the steady intensities of filtered fields.

In our scheme, as illustrated in Fig. 1, the quantum emitter is a Λ-type system consisting of an excited state denoted by $|3\rangle$ coupled with lower nondegenerate states $|1\rangle$ and $|2\rangle$. Two monochromatic lasers of frequencies ω_1, ω_2 are applied to drive the electronic dipole-allowed transitions $|3\rangle \to |1\rangle$ and $|3\rangle \to |2\rangle$, separated by the level splittings ω_{31} and ω_{32}, with Rabi frequencies Ω_1, Ω_2, respectively. At the same time, the driven transition $|3\rangle \to |1\rangle(|2\rangle)$ is also coupled to two cavity modes with frequencies $\omega_{a_1}, \omega_{a_2}(\omega_{b_1}, \omega_{b_2})$, labeled by their annihilation operators $a_1, a_2(b_1, b_2)$.

Working in the frame rotating with respect to the driving laser frequencies ω_1 and ω_2, the time evolution of the hybrid quantum system is governed by the master equation of density operator ρ in the dipole approximation and rotating wave approximation [57]

$$\frac{d\rho}{dt} = -\frac{i}{\hbar}[H, \rho] + \mathcal{L}\rho, \tag{4}$$

in which the total Hamiltonian of the hybrid quantum system can be decomposed into three parts $H = H_{AL} + H_C + H_{AC}$, where

$$\begin{aligned} H_{AL} &= \hbar \sum_{l=1,2} [-\Delta_l \sigma_{ll} + \Omega_l(\sigma_{3l} + \sigma_{l3})], \\ H_C &= \hbar \sum_{l=1,2} \Delta_{a_l} a_l^\dagger a_l + \hbar \sum_{l=1,2} \Delta_{b_l} b_l^\dagger b_l, \\ H_{AC} &= \hbar \sum_{l=1,2} (g_{a_l} a_l^\dagger \sigma_{13} + g_{b_l} b_l^\dagger \sigma_{23}) + \text{H.c.}. \end{aligned} \tag{5}$$

The first part, H_{AL}, describes the unperturbed energy of the atom and its dipolar interactions with two classical driving fields. The operators $\sigma_{kk'} = |k\rangle\langle k'|(k, k' = 1, 2, 3)$ are the population operators for $k = k'$ and atomic flip operators for $k \neq k'$. $\Delta_l (l = 1, 2)$ are the detunings of the atomic transition frequencies from the laser fields by which they are driven, i.e., $\Delta_l = \omega_{3l} - \omega_l$. The other two parts, H_C and H_{AC}, describe the free Hamiltonian of four-mode quantized cavity fields and the couplings between cavity modes and atomic transitions, respectively. The parameters $\Delta_{a_l} = \omega_{a_l} - \omega_1$, $\Delta_{b_l} = \omega_{b_l} - \omega_2$ are the detunings between the cavity modes and corresponding applied fields. g_{a_l} (g_{b_l}) are the coupling constants between the cavity modes $a_l(b_l)$ and atomic transition $|3\rangle \leftrightarrow |1\rangle(|2\rangle)$. The last term $\mathcal{L}\rho = \mathcal{L}_A\rho + \mathcal{L}_C\rho$ in Eq. (4) denotes the atomic dissipation to the background environment besides the privileged cavity modes, and the dissipation of the cavity modes, which take the form

$$\begin{aligned} \mathcal{L}_A\rho &= \sum_{l=1,2} \frac{\gamma_l}{2} \mathcal{D}[\sigma_{l3}]\rho, \\ \mathcal{L}_C\rho &= \sum_{l=1,2} \left(\frac{\kappa_{a_l}}{2} \mathcal{D}[a_l]\rho + \frac{\kappa_{b_l}}{2} \mathcal{D}[b_l]\rho \right), \end{aligned} \tag{6}$$

respectively, where $\mathcal{D}[\mathcal{O}]\rho = [\mathcal{O}\rho, \mathcal{O}^\dagger] + [\mathcal{O}, \rho\mathcal{O}^\dagger]$ is the Lindblad-type superoperator. The parameters γ_l are the atomic decay rates from $|3\rangle$ to $|l\rangle$, and κ_{a_l}, κ_{b_l} are the decay rates of the cavity modes a_l, b_l, respectively. We assume that the Rabi frequencies are equal for the sake of simplicity, and by working in the strong excitation regime, i.e., $\Omega_l = \Omega \gg (\gamma_l, \kappa_i)$ $(i = a_l, b_l$ with $l = 1, 2)$, that the fluorescent spectrum can be decomposed into individual emission lines, it is enlightening to introduce semiclassical dressed bases [58]

$$\begin{pmatrix} |1_A\rangle \\ |2_A\rangle \\ |3_A\rangle \end{pmatrix} = \begin{pmatrix} \frac{1-\sin\theta}{2} & \frac{1+\sin\theta}{2} & -\frac{\cos\theta}{\sqrt{2}} \\ -\frac{\cos\theta}{\sqrt{2}} & \frac{\cos\theta}{\sqrt{2}} & \sin\theta \\ \frac{1+\sin\theta}{2} & \frac{1-\sin\theta}{2} & \frac{\cos\theta}{\sqrt{2}} \end{pmatrix} \begin{pmatrix} |1\rangle \\ |2\rangle \\ |3\rangle \end{pmatrix}, \tag{7}$$

where $\sin\theta = \Delta/\bar{\Omega}$, $\cos\theta = \sqrt{2}\Omega/\bar{\Omega}$, and we have already assumed $\Delta_2 = -\Delta_1 = \Delta$. The parameter $\bar{\Omega} = \sqrt{\Delta^2 + 2\Omega^2}$ is the generalized Rabi frequency involving the separations of two adjacent levels in each dressed triplet. In order to choose spectral lines of interest, it is beneficial to divide the atomic operators into several dressed components defined as $\tilde{\sigma}_{kk'} = |k_A\rangle\langle k'_A|(k, k' = 1, 2, 3)$

$$\sigma_{l3} = \sigma_{S_2}^{(l)} + \sigma_{S_1}^{(l)} + \sigma_R^{(l)} + \sigma_{A_1}^{(l)} + \sigma_{A_2}^{(l)}, \tag{8}$$

in which $\sigma_{A_1}^{(1)} = -A\tilde{\sigma}_{23} + B_-\tilde{\sigma}_{12}$ and $\sigma_{S_1}^{(1)} = A\tilde{\sigma}_{21} + B_+\tilde{\sigma}_{32}$ dominate the fluorescent emissions of the higher-frequency inner sideband with frequency $\omega_1 + \bar{\Omega}$ and lower-frequency inner sideband with frequency $\omega_1 - \bar{\Omega}$, respectively, in a resonance fluorescence spectrum generated from emission $|3\rangle \to |1\rangle$, where the parameters $A = (\cos^2\theta)/2$, $B_\pm = \sin\theta(1 \pm \sin\theta)/2$ are the transition amplitudes between the corresponding dressed states. These two components of fluorescence are selected to be injected into the target cavity 1 and cavity 2 to trigger quantum modes in a_1 and a_2. Similarly, $\sigma_{A_1}^{(2)} = A\tilde{\sigma}_{23} + B_+\tilde{\sigma}_{12}$ and $\sigma_{S_1}^{(2)} = -A\tilde{\sigma}_{21} + B_-\tilde{\sigma}_{32}$ give rise to another higher-frequency inner sideband and lower-frequency inner sideband from $|3\rangle \to |2\rangle$, and pump cavity 3 with mode b_1 and cavity 4 with mode b_2, respectively. The operators $\sigma_R^{(l)}$ describe the spontaneous emission of dressed atom between two same dressed levels of two adjacent triplets and give rise to the Rayleigh spectral lines located at driving frequencies ω_l. The remaining components $\sigma_{S_2}^{(l)}$ and $\sigma_{A_2}^{(l)}$ generate two outer sidebands. It is worth noting that, under strong excitation regime, each Lorentzian cavity can be activated only when

its frequency is tuned near the center frequency of its target spectral line, so the coupling far away from the resonance can be ignored. In addition, the existence of each cavity merely decorates the density of vacuum modes at which it is located into the Lorenzian type, and almost do not impact the vacuum environment that the driven atom feels, i.e., the standard dissipations described by Eq. (6) are still valid [59]. Meanwhile, with the help of secular approximation, the atomic dissipation in Eq. (6) can be decomposed into the superposition of dissipations in several dressed transition channels by dropping other fast-rotating terms [34].

In this interaction system, as mentioned in the above, each coupling constant is required to be small enough, i.e., $g_i \ll \sqrt{\gamma_l \kappa_i}$ [41], so that the fluorescence filtering can be felicitously equivalent to perturbation to the quantum emitter. Ingeniously, all coupling constants disappear algebraically from our final analytic results.

III. TEMPORAL INTENSITY CORRELATIONS WITH LARGE FILTER WIDTHS

In this paper, we are mainly interested in the filtering processes with large filter passband widths (bad cavity limit) specified as $\kappa_i \gg \gamma_l \gg g_i$, in which each target spectral line can be covered completely by the sweep range of the corresponding filter in frequency domain, ensuring that all the photons coming from the target spectral line can be captured uniformly [34]. In the following discussion, we temporarily assume $\kappa_i = \kappa$, $g_i = g$, and $\gamma_l = \gamma$.

A. Conditional state and preferred selection for time orderings

We first correlate two filtered photons in mode a_1 and a_2, respectively, which are radiated from a common dipole-allowed transition $|3\rangle \to |1\rangle$. Considering the measurement for a_1 at time t in the stationary dynamics followed by the second counting at later time $t+\tau(\tau > 0)$ for a_2, the unnormalized two-photon correlation can be expressed as $\mathcal{G}^{(2)}(a_1, a_2, \tau) = \mathrm{Tr}[a_2^\dagger a_2 \rho^r(\tau)]$, where $\rho^r(\tau)$ is the conditioned (collapsed) state of the composite system prepared by the preselection. According to the principle of photoelectric counting, the intensity of incident field is very weak so that each filter passes through only one photon at a time [60]. Therefore, we may consider the dynamics of quantum system in a Hilbert space truncated at single-photon excitation manifold for each cavity mode. This suggests that, after preselection, only cavity photon a_2 may survive in the bad cavity. In this case, the conditioned state ρ^r at time t can be factorized as $\rho^r = \rho^r_{A,a_2} \otimes \rho^r_{a_1}$, in which $\rho^r_{a_1} \equiv |0_{a_1}\rangle\langle 0_{a_1}|$, and ρ^r_{A,a_2}, the point of departure for our analysis, is the reduced density operator of subsystem composed of dressed atom photons in field a_2, and turns out to be the incoherent superposition of three orthogonal pure states as

$$\begin{aligned}\rho^r_{A,a_2} = {} & \langle\tilde{\sigma}_{11}\rangle_s |\mathcal{C}_{1,1}|^2 |1_A, 1_{a_2}\rangle\langle 1_A, 1_{a_2}| \\ & + \mathcal{I}_2^{(a_1)}\big(|1_A, 0_{a_2}\rangle + \mathcal{C}_{2,1}|2_A, 1_{a_2}\rangle\big) \\ & \times \big(\langle 1_A, 0_{a_2}| + \mathcal{C}^*_{2,1}\langle 2_A, 1_{a_2}|\big) \\ & + \mathcal{I}_3^{(a_1)}\big(|2_A, 0_{a_2}\rangle + \mathcal{C}_{3,1}|3_A, 1_{a_2}\rangle\big) \\ & \times \big(\langle 2_A, 0_{a_2}| + \mathcal{C}^*_{3,1}\langle 3_A, 1_{a_2}|\big), \end{aligned} \tag{9}$$

where $\mathcal{I}_2^{(a_1)}$ and $\mathcal{I}_3^{(a_1)}$ are the two components of the average photon number for cavity mode a_1 (filtered intensity of the higher-frequency inner sideband of resonance fluorescent field) contributed from two steady dressed populations $\langle\tilde{\sigma}_{22}\rangle_s$ and $\langle\tilde{\sigma}_{33}\rangle_s$, respectively, i.e., $\langle a_1^\dagger a_1\rangle_s = \mathcal{I}_2^{(a_1)} + \mathcal{I}_3^{(a_1)}$, with

$$\mathcal{I}_2^{(a_1)} = \frac{g^2 B_-^2 \langle\tilde{\sigma}_{22}\rangle_s}{\left(\frac{\kappa}{2}\right)^2 + \delta_{a_1}^2}, \quad \mathcal{I}_3^{(a_1)} = \frac{g^2 A^2 \langle\tilde{\sigma}_{33}\rangle_s}{\left(\frac{\kappa}{2}\right)^2 + \delta_{a_1}^2}, \tag{10}$$

where the parameters δ_{a_l} and δ_{b_l} (which will be shown later) are the filter detunings from the central frequencies of their target spectral lines, i.e., $\delta_{a_1} = \omega_{a_1} - (\omega_1 + \bar{\Omega})$, $\delta_{a_2} = \omega_{a_2} - (\omega_1 - \bar{\Omega})$, $\delta_{b_1} = \omega_{b_1} - (\omega_2 + \bar{\Omega})$, and $\delta_{b_2} = \omega_{b_2} - (\omega_2 - \bar{\Omega})$. In the limit of short time difference $\tau \ll \gamma^{-1}$, Eq. (9) suggests that, conditioned on the preselection for photon a_1, the total probability of capturing a photon a_2 is the sum of the components of probability $|\mathcal{C}_{1,1}(\tau)|^2$, $|\mathcal{C}_{2,1}(\tau)|^2$, and $|\mathcal{C}_{3,1}(\tau)|^2$. Performing lengthy but straightforward calculations, the conditional probability amplitudes can be expressed as

$$\begin{aligned} \mathcal{C}_{2,1}(\tau) &= \mathcal{F}_{22}^{(a_2),+}(\tau) + \mathcal{F}_{22}^{(a_2),-}(\tau), \\ \mathcal{C}_{3,1}(\tau) &= \mathcal{F}_{33}^{(a_2),+}(\tau), \\ \mathcal{C}_{1,1}(\tau) &= \mathcal{T}_{11}^{(a_1 a_2),-}(\tau). \end{aligned} \tag{11}$$

Here, we introduce the general forms of conditional single-photon emission amplitudes for positive time ordering and reverse time ordering

$$\mathcal{F}^+(\delta_1, \delta_2, \tau) = \frac{1}{\frac{\kappa}{2} + i\delta_2}\left[1 - \frac{\left(\frac{\kappa}{2} + i\delta_1\right)e^{-(\frac{\kappa}{2} + i\delta_2)\tau}}{\kappa + i(\delta_1 + \delta_2)}\right], \tag{12}$$

$$\mathcal{F}^-(\delta_1, \delta_2, \tau) = \frac{\left(\frac{\kappa}{2} + i\delta_1\right)e^{-(\frac{\kappa}{2} + i\delta_2)\tau}}{\left(\frac{\kappa}{2} + i\delta_2\right)[\kappa + i(\delta_1 + \delta_2)]}, \tag{13}$$

respectively, to describe the situation that the order of two-photon emission is corresponding to the given order of detection, and the concomitant opposite situation. Meanwhile, the two-photon joint emission amplitude for reverse time ordering

$$\mathcal{T}^-(\delta_1, \delta_2, \tau) = \frac{e^{-(\frac{\kappa}{2} + i\delta_2)\tau}}{\left(\frac{\kappa}{2} + i\delta_2\right)[\kappa + i(\delta_1 + \delta_2)]} \tag{14}$$

is also introduced to describe the isolated reverse time ordering. Then, the detailed expressions of the time ordering amplitudes in Eq. (11) can be given compactly as

$$\begin{aligned} \mathcal{F}_{22}^{(a_2),+}(\tau) &= -igA\mathcal{F}^+\big(\delta_{a_1}, \delta_{a_2}, \tau\big), \\ \mathcal{F}_{22}^{(a_2),-}(\tau) &= ig\frac{AB_+}{B_-}\mathcal{F}^-\big(\delta_{a_1}, \delta_{a_2}, \tau\big), \\ \mathcal{F}_{33}^{(a_2),+}(\tau) &= -igB_+\mathcal{F}^+\big(\delta_{a_1}, \delta_{a_2}, \tau\big), \\ \mathcal{T}_{11}^{(a_1 a_2),-}(\tau) &= gAB_-\mathcal{T}^-\big(\delta_{a_1}, \delta_{a_2}, \tau\big). \end{aligned} \tag{15}$$

With these definitions, $\mathcal{G}^{(2)}(a_1, a_2, \tau)$ is written compactly as

$$\begin{aligned}\mathcal{G}^{(2)}(a_1, a_2, \tau) = {} & \mathcal{I}_2^{(a_1)}\big|\mathcal{F}_{22}^{(a_2),+}(\tau) + \mathcal{F}_{22}^{(a_2),-}(\tau)\big|^2 \\ & + \mathcal{I}_3^{(a_1)}\big|\mathcal{F}_{33}^{(a_2),+}(\tau)\big|^2 + \langle\tilde{\sigma}_{11}\rangle_s\big|\mathcal{T}_{11}^{(a_1 a_2),-}(\tau)\big|^2. \end{aligned} \tag{16}$$

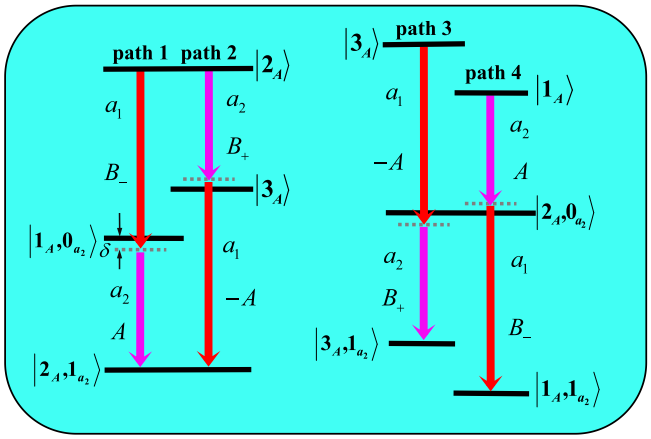

FIG. 2. Transition paths and time orderings of two-photon resonant cascaded emissions of photon pair (a_1, a_2), in which path 1 and path 2 display interference involving a common initial dressed state and a final dressed state $|2_A\rangle$, and path 3 and path 4 are independent time ordering channels. Red and pink arrows represent the photon emissions in mode a_1 and a_2, respectively. The relative transition amplitudes, A, B_+, and B_-, are labeled.

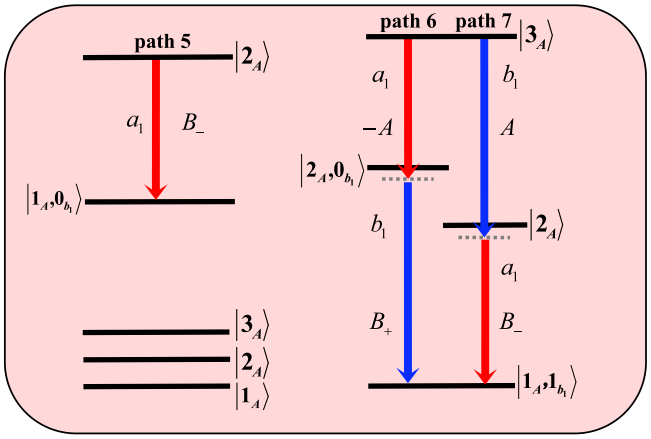

FIG. 3. Transition paths and time orderings of two-photon nonresonant cascaded emissions of photon pair (a_1, b_1), which relate to the pure interference of time orderings described by path 6 and path 7. Red and blue arrows represent the photon emissions in mode a_1 and b_1, respectively. The relative transition amplitudes, A, B_+, and B_-, are also labeled.

Physically, $\mathcal{F}_{ij}^{(a_2),+}(\tau)$ can be understood as the conditional time ordering transition amplitude of photon a_2 originating from the two-photon cascaded emission with the order of emission corresponding to the order of detection when the dressed atom starts from the initial state $|i_A\rangle$ to the target state $|j_A\rangle$. Whereas, $\mathcal{F}_{ij}^{(a_2),-}(\tau)$ accounts for the emission amplitude that photon a_2 emitted before a_1, describing the reverse process. The amplitude $\mathcal{T}_{ij}^{(a_1a_2),-}(\tau)$ directly describes the independent two-photon successive transition with ordering of emission opposite to the orderings of detection. With the help of the conditioned state in Eq. (9), we may grasp the physical insight into the time orderings from the three parts of two-mode correlation in Eq. (16), as shown in Fig. 2. In path 1, after emitting a photon a_1 from the initial state $|2_A\rangle$, the dressed atom basically rests on the state $|1_A\rangle$ after preselection. However, there is a small probability that two photons a_1, a_2 have been prepared in cavities and photon a_2 still survives after a_1 is annihilated. In addition, another alternative two-photon path 2 also gives rise to the two-photon emission with the reverse time ordering, thus the total probability amplitude of finding photon a_2 is the superposition of this two transition paths. Correspondingly, if the dressed atom starts from the initial state $|3_A\rangle$, two photons are generated from the positive time ordering described by $\mathcal{C}_{3,1}(\tau) = \mathcal{F}_{33}^{(a_2),+}(\tau)$ accounting for path 3. Whereas, the dressed state $|1_A\rangle$ only gives rise to the isolated reverse time ordering process in path 4, which should be directly depicted by the two-photon joint emission $\mathcal{C}_{1,1}(\tau) = \mathcal{T}_{11}^{(a_1a_2),-}(\tau)$. Interestingly, despite the fact that two different successive emissions, sharing a common initial state and a common final state $|2_A\rangle$, display interference, it can be noticed that the dressed atom is more likely to be selectively trapped in the intermediate state belonging to positive time ordering (path 1), which is preferentially selected by the filter-detector system.

For another situation that cavity photon a_1 is probed at t followed by the counting of b_1 at a later time $t + \tau$, the unnormalized conditioned state for dressed atom-photon b_1 prepared by the first detection is also found as

$$\rho_{A,b_1}^r = \mathcal{I}_3^{(a_1)}\big(|2_A, 0_{b_1}\rangle + \mathcal{C}'_{1,1}|1_A, 1_{b_1}\rangle\big) \times \big(\langle 2_A, 0_{b_1}| + \mathcal{C}'^*_{1,1}\langle 1_A, 1_{b_1}|\big) + \mathcal{I}_2^{(a_1)}|1_A, 0_{b_1}\rangle\langle 1_A, 0_{b_1}|. \tag{17}$$

Correspondingly, the unnormalized two-mode correlation function for short delay can be expressed as

$$\mathcal{G}_s^{(2)}(a_1, b_1, \tau) = \mathcal{I}_3^{(a_1)}|\mathcal{C}'_{1,1}(\tau)|^2 = \mathcal{I}_3^{(a_1)}\big|\mathcal{F}_{31}^{(b_1),+}(\tau) + \mathcal{F}_{31}^{(b_1),-}(\tau)\big|^2, \tag{18}$$

where the conditional emission amplitudes for positive time ordering and reverse time ordering are given, respectively, by

$$\begin{aligned}\mathcal{F}_{31}^{(b_1),+}(\tau) &= -igB_+\mathcal{F}^+\big(\delta_{a_1}, \delta_{b_1}, \tau\big),\\ \mathcal{F}_{31}^{(b_1),-}(\tau) &= igB_-\mathcal{F}^-\big(\delta_{a_1}, \delta_{b_1}, \tau\big).\end{aligned} \tag{19}$$

Obviously, the structures of conditioned state and two-mode correlation function in this situation are different from the former, which is the consequence of nonresonant two-photon cascaded emissions ($\omega_{a_1} + \omega_{b_1} \neq 2\omega_L$). As the path 5 in Fig. 3, starting from the dressed level $|2_A\rangle$, the dressed atom is prepared at $|1_A\rangle$ by converting a pumping photon with frequency ω_1 into a cavity photon a_1. In addition, this conversion can also be realized alternatively from $|3_A\rangle$ to $|2_A\rangle$ in path 6. When a_1 is detected, these two possible single-photon paths give rise to the states $|1_A, 0_{b_1}\rangle$ and $|2_A, 0_{b_1}\rangle$. Unfortunately, for generating photon b_1, only the initial state $|3_A\rangle$ is able to complete two-photon preparation via the positive time ordering (path 6) or its adjoint reverse time ordering (path 7).

For the third group of fluorescent photons, photon a_1 and b_2 weakly driving cavity 1 and cavity 4, respectively, are also correlated for completeness, in which a_1 is detected at first at time t. The unnormalized two-mode correlation signal can

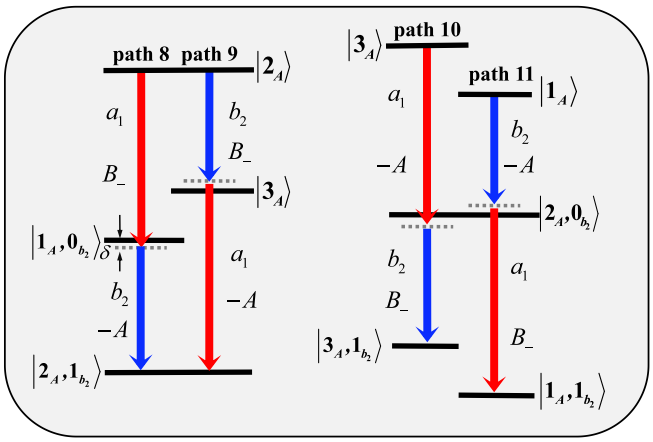

FIG. 4. Transition paths and time orderings of two-photon resonant cascaded emissions of photon pair (a_1, b_2), which are the same as photon pair (a_1, a_2) except for one of the relative transition amplitudes for field b_2. Red and blue arrows represent the photon emissions in mode a_1 and b_2, respectively. The relative transition amplitudes, A and B_-, are also labeled.

also be calculated based on the same process as before, and then we arrive at

$$\mathcal{G}^{(2)}(a_1, b_2, \tau) = \mathcal{I}_2^{(a_1)}\left|\mathcal{F}_{22}^{(b_2),+}(\tau) + \mathcal{F}_{22}^{(b_2),-}(\tau)\right|^2 + \mathcal{I}_3^{(a_1)}\left|\mathcal{F}_{33}^{(b_2),+}(\tau)\right|^2 + \langle\tilde{\sigma}_{11}\rangle_s\left|\mathcal{T}_{11}^{(a_1 b_2),-}(\tau)\right|^2 \tag{20}$$

with the conditional emission amplitudes

$$\begin{aligned}
\mathcal{F}_{22}^{(b_2),+}(\tau) &= igA\mathcal{F}^+(\delta_{a_1}, \delta_{b_2}, \tau),\\
\mathcal{F}_{22}^{(b_2),-}(\tau) &= igA\mathcal{F}^-(\delta_{a_1}, \delta_{b_2}, \tau),\\
\mathcal{F}_{33}^{(b_2),+}(\tau) &= -igB_-\mathcal{F}^+(\delta_{a_1}, \delta_{b_2}, \tau),\\
\mathcal{T}_{11}^{(a_1 b_2),-}(\tau) &= -gAB_-\mathcal{T}^-(\delta_{a_1}, \delta_{b_2}, \tau).
\end{aligned} \tag{21}$$

It is not difficult to observe that this group of photon pair is consistent with the first one (a_1, a_2) in time orderings, the only difference is that one of the transition amplitudes of mode b_2 is different from that of photon a_2, as shown in Fig. 4. Therefore, there is a simple correspondence and substitution of transition amplitudes, leading to the similarity of time orderings between (a_1, a_2) and (a_1, b_2).

So far, we have obtained the two-mode correlations with perspicuity physically pictured in terms of conditional time ordering amplitudes, which are the product of cavity mode detection theory. In our approach, we inspect time orderings from the conditioned state prepared by the first photon detection, instead of directly prejudging time orderings by permuting original atomic dipole operators before detecting first photon. However, the information of time orderings is preserved effectively and expressed skillfully through the time ordering amplitudes. As we expected, after straightforward algebraic arrangement, Eq. (16), (18), and (20) reproduce the analytical forms given by the early fundamental method of two-photon detection operator established by Nienhuis *et al.* [34].

B. Past quantum state and collective monitoring

In this section, we supplement the two-mode correlations by the recent past quantum state formalism to trace back to the conditioned dynamics involving time orderings conditioned by the final detection [49].

Considering the photon pairs (a_1, a_2), if the later detector probes a filtered photon a_1 at a given time t, one may wonder what scenery the two filter-detector systems have experienced at earlier times until the first detection for photon a_2 at $t + \tau$ $(\tau < 0)$? Based on the spirit of past quantum state formalism of positive operator valued measurement, two-mode quantum correlation between different times can be established from the given final time t backwards to the past time $t + \tau$ through the reverse evolution operator $E_{a_1}(\tau) = U^\dagger(t, t+\tau)a_1^\dagger a_1 U(t, t+\tau)$. It solves the reverse evolution equation $dE_{a_1}(t) = \frac{i}{\hbar}[H, E_{a_1}]dt + \frac{\kappa}{2}(\mathcal{D}^\dagger[a_1]E_{a_1} + \mathcal{D}^\dagger[a_2]E_{a_1})dt$, where $dt = (t + dt) - t$, whereas the anomalous definition for $dE = E(t - dt) - E(t)$ is introduced because of inverse evolution. The first term of Lindblad operator for $\rho(t)$ should be restored to the pumping process for $E(t)$, i.e., $\mathcal{D}^\dagger[a_l]E = 2a_l^\dagger E a_l - a_l^\dagger a_l E - E a_l^\dagger a_l$ [61–63]. Until time $t + \tau$, the monitored subsystem has been prepared to $\rho^r_{A,a_2} = a_2\rho a_2^\dagger$ by the preselection, this leads to the unnormalized cross-correlation $\mathcal{G}^{(2)}(a_1, a_2, \tau < 0) = \mathrm{Tr}[\rho^r_{A,a_2}E_{a_1}(\tau)]$. After entering the truncated Hilbert space, one yields the reverse evolution operator E_{a_1} for short delay as follows:

$$\begin{aligned}
E_{a_1}(\tau) = {} & |\mathcal{E}_{3,1}(\tau)|^2\left|3_A, 1_{a_1}\right\rangle\left\langle 3_A, 1_{a_1}\right|\\
& + \left(\mathcal{E}_{2,0}(\tau)\left|2_A, 0_{a_1}\right\rangle + \mathcal{E}_{1,1}(\tau)\left|1_A, 1_{a_1}\right\rangle\right)\\
& \times \left(\mathcal{E}^*_{2,0}(\tau)\left\langle 2_A, 0_{a_1}\right| + \mathcal{E}^*_{1,1}(\tau)\left\langle 1_A, 1_{a_1}\right|\right)\\
& + \left(\mathcal{E}_{3,0}(\tau)\left|3_A, 0_{a_1}\right\rangle + \mathcal{E}_{2,1}(\tau)\left|2_A, 1_{a_1}\right\rangle\right)\\
& \times \left(\mathcal{E}^*_{3,0}(\tau)\left\langle 3_A, 0_{a_1}\right| + \mathcal{E}^*_{2,1}(\tau)\left\langle 2_A, 1_{a_1}\right|\right),
\end{aligned} \tag{22}$$

with the time-dependent coefficients

$$\begin{aligned}
|\mathcal{E}_{3,1}(\tau)|^2 &= e^{\kappa\tau},\\
\mathcal{E}_{1,1}(\tau) &= \mathcal{E}_{2,1}(\tau) = e^{(\frac{\kappa}{2} - i\delta_{a_1})\tau},\\
\mathcal{E}_{2,0}(\tau) &= \frac{igB_-}{\frac{\kappa}{2} - i\delta_{a_1}}\left[1 - e^{(\frac{\kappa}{2} - i\delta_{a_1})\tau}\right],\\
\mathcal{E}_{3,0}(\tau) &= \frac{-igA}{\frac{\kappa}{2} - i\delta_{a_1}}\left[1 - e^{(\frac{\kappa}{2} - i\delta_{a_1})\tau}\right].
\end{aligned} \tag{23}$$

It is straightforward to confirm that, after some algebraic processing, the quantum past state approach reproduce the same quantitative prediction for two-mode correlation in Eq. (16) given by the conditional time ordering emission amplitudes. Starting from Eq. (22) to trace back to the information of past quantum state, the form of E_{a_1} indicates that although the quantum system is prepared by the preselection, the effect of postselection consummates the past knowledge that probed quantum system evolves guided by the later monitoring system, and collapse to the target state $|1_A, 1_{a_1}\rangle$, $|2_A, 1_{a_1}\rangle$, and $|3_A, 1_{a_1}\rangle$ expectably, regressing E_{a_1} to unit operator [49]. This historical dynamics may not be exhibited by the forward evolution from preselection which displays the spontaneous evolution dominated by $e^{\mathcal{L}\tau}$ of unobserved quantum

system ($\frac{d\rho}{d\tau} = e^{\mathscr{L}\tau}\rho$) and waiting to be measured by the later monitoring system. Moreover, we prefer to consider that it is the later monitoring system that guides the evolution of dressed atom-photon system with the ordering of emission corresponding to the ordering of detection. In other words, it is the collective effect of two monitoring systems that establish the correlation between photon a_2 in the past and a_1 at present. When the order of detection is given, the later monitoring system induces the evolution of quantum system and shrinks the wave packet into the final target states $|1_A, 1_{a_1}\rangle$, $|2_A, 1_{a_1}\rangle$, and $|3_A, 1_{a_1}\rangle$, in which the past initial state is prepared by the preselection performed by the former one.

We would like to finish this section with a brief summary of the effect of monitoring systems for quantum system in FRC, preferred selection for time orderings and collective monitoring. In detail, on the one hand, the former monitoring system preferentially select positive time ordering channels from quantum emitter and collapse it into the intermediate states belonging to the paths with positive emission ordering, regardless of the existence of interference between two opposite time orderings. On the other hand, conditioned on the postselection, it is the later monitoring system that induces the probed quantum system into the target state through its weak coupling interaction with quantum emitter. It is also worth emphasizing that the compact forms of the conditioned states and correlation functions can only be maintained in the limit of short delay, and the time orderings can only be identified in this limit. This forms are subverted by the atomic spontaneous decay for long time difference. The explicit analytic expression of two-mode correlation function for arbitrary time delay are shown in Appendix B, which can return to the simple result given by the color-blind filters ($\lambda \to \infty$) [19,34,41].

IV. TIME ORDERING ROUTING AND CONTROLLING

In this section, we concentrate on the features of second-order correlation signals, and discuss in detail the feasibility of controlling the privileged temporal correlations with the comparison of the obtained results in two-level atom and four-level quantum dot modeled by a three-level ladder system.

A. Resonant two-photon cascaded emissions

We first investigate the paired photons (a_1, a_2) and (a_1, b_2), whose frequencies obey the resonant cascaded two-photon processes $\omega_{a_1} + \omega_{a_2} = 2\omega_1$ and $\omega_{a_1} + \omega_{b_2} = \omega_1 + \omega_2$, i.e., the filter detunings satisfy the relation $\delta_{a_1} = -\delta_{a_2} = -\delta_{b_2} = \delta$. Figures 5(a) and 5(b) present the normalized second-order correlation signals $g^{(2)}(a_1, a_2)$ and $g^{(2)}(a_1, b_2)$ for arbitrary delay and laser detuning with the parameters $\Omega = 100\gamma$, $\kappa = 20\gamma$, and $\delta = 0$. From the result of (a_1, a_2), photon pairs display bunching behavior for delay measurements, and the symmetry of $g^{(2)}(a_1, a_2, \tau)$ is sensitive to the laser detuning, which can be further noticed from Figs. 5(c) and 5(d). Whereas, the correlation of (a_1, b_2) is symmetric in time domain, and robust to the laser detuning. The bunching for both positive and negative delays in photon pair (a_1, a_2) stems from the simultaneous appearance of two differentiable dressed state transition amplitudes B_+, B_- in two different two-photon resonant cascaded channels both with positive

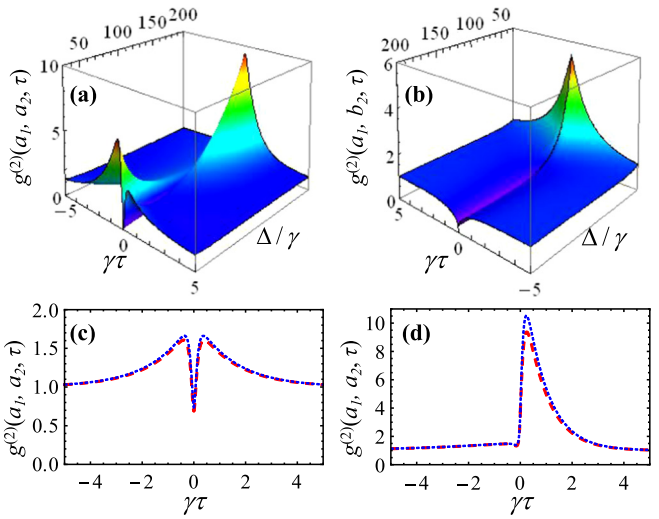

FIG. 5. Normalized second-order correlation signals (a) $g^{(2)}(a_1, a_2, \tau)$ and (b) $g^{(2)}(a_1, b_2, \tau)$, as functions of arbitrary delay τ and laser detuning Δ for $\Omega = 100\gamma$, $\kappa = 20\gamma$ and $\delta = 0$. (c) and (d) are the intersecting surfaces of (a) at $\Delta = 100\gamma$ and $\Delta = 200\gamma$, in which the red dashed thick lines and blue dashed thin lines represent the analytical results and numerical results without large width approximation, respectively.

time ordering and the other two different channels both with reverse time ordering. It is easy to verify that $\langle\tilde{\sigma}_{11}\rangle_s = \langle\tilde{\sigma}_{22}\rangle_s = \langle\tilde{\sigma}_{33}\rangle_s$ for $\Delta = \pm\Omega$, but $|B_+| > |B_-|$, the contribution of two-photon path 3 in Fig. 2 is dominant in the value of $g^{(2)}(a_1, a_2, \tau > 0)$ [green dashed thin line in Fig. 6(b)].

If the detection orderings are exchanged, the transition amplitude B_+ can still enhance its positive time ordering in path 2, giving rise to the large contribution of $g^{(2)}(a_1, a_2, \tau < 0)$ [red dot-dashed thick line in Fig. 6(b)]. As a consequence, two opposite detection orderings both possess their corresponding dominant positive time ordering and exhibit symmetric correlation signal. However, this symmetry can be broken by the maldistribution of dressed populations. For example, for $\Delta = 30\gamma$, $\langle\tilde{\sigma}_{22}\rangle_s \approx 20\langle\tilde{\sigma}_{11}\rangle_s$ and $|B_+| \approx 1.52|B_-|$, triggering the projecting path 2 with large probability, so the correlation for negative delay is stronger than positive, as shown in Fig. 5(a). Similarly, if $\Delta > \Omega$, for example $\Delta = 200\gamma$, it leads to $\langle\tilde{\sigma}_{11}\rangle_s = \langle\tilde{\sigma}_{33}\rangle_s \approx 10\langle\tilde{\sigma}_{22}\rangle_s$ and $|B_+| \approx 10|B_-|$, then, path 3 being the positive time ordering of $\tau > 0$ is significantly protruded, as shown in Fig. 5(d).

On the other hand, for photon pairs (a_1, b_2), all the two-photon cascaded paths are related to the dressed transition amplitudes A and B_-, consequently, all the possible two-photon cascaded emissions without protruded time ordering lead to the ambiguity of time orderings and give rise to the identical results for two opposite detection orderings regardless of distribution of dressed populations, as long as the delays are equal, as illustrated in Fig. 5(b). Interestingly, it is enlightening to recall the situation of opposite sidebands in Mollow triplet, in which the time-dependent two-photon spectral correlation is also symmetric under resonant excitation due to equal dressed populations.

In Figs. 5(c) and 5(d), apart from the obtained analytical results depicted by the red dashed thick lines, the numerical

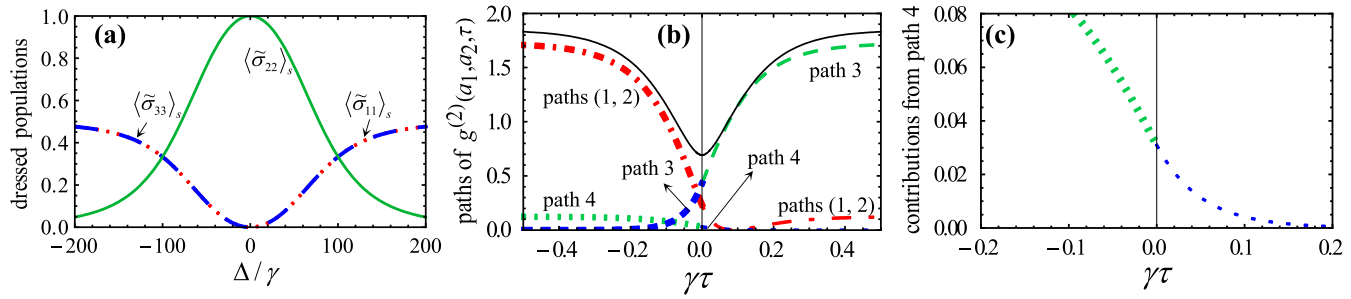

FIG. 6. (a) Steady dressed populations $\langle\tilde{\sigma}_{11}\rangle_s$ (red dotted line), $\langle\tilde{\sigma}_{22}\rangle_s$ (green solid line), and $\langle\tilde{\sigma}_{33}\rangle_s$ (blue dashed line). (b) The value of $g^{(2)}(a_1, a_2, \tau)$ in Fig. 5 (c) is decomposed, in which the red dot-dashed thin line, green dashed thin line, and blue dotted thin line correspond to the contributions from paths (1, 2), path 3, and path 4 for $\tau > 0$, and the red dot-dashed thick line, green dotted thick line, and blue dashed thick line represent the contributions from paths (1, 2), path 4, and path 3 for $\tau < 0$, respectively. The total normalized correlation function $g^{(2)}(a_1, a_2, \tau)$ is plotted by the black solid thin line (top), which is the sum of the above three parts. (c) Enlarged view of the contributions from path 4 to $g^{(2)}(a_1, a_2, \tau)$ in (b). Its contributions for $\tau > 0$ and $\tau < 0$ are depicted by the blue dotted thin line and green dotted thick line, respectively.

results of $g^{(2)}(a_1, a_2, \tau)$ and $g^{(2)}(a_1, b_2, \tau)$ without large filter width approximation are also presented by the blue dashed thin lines. In our numerical calculations, all the correlation functions can be obtained from its equations of motion, which are coupled to other related terms. In this series of equations of motion, even in the case of large filter widths, all the linear terms of atomic spontaneous emission rates are preserved, making it difficult to solve steady-state correlation signals. The detailed and further descriptions of numerical method are demonstrated in Appendix A. However, fortunately, if all the terms involving atomic spontaneous emission are neglected, the steady-state solution of each coupled equation and correlation signals can be obtained analytically and give rise to the red dashed thick lines in Figs. 5(c) and 5(d) [and Figs. 8(a)–8(h) in the following].

B. Nonresonant two-photon cascaded emissions

We now turn to other paired photons (a_1, b_1) whose frequencies do not satisfy the energy conservation with two pumping photons ($\omega_{a_1} + \omega_{b_1} \neq \omega_1 + \omega_2$), because there exists only two possible two-photon cascaded paths $|3_A\rangle \xrightarrow{\Omega_1,a_1} |2_A\rangle \xrightarrow{\Omega_2,b_1} |1_A\rangle$ and $|3_A\rangle \xrightarrow{\Omega_2,b_1} |2_A\rangle \xrightarrow{\Omega_1,a_1} |1_A\rangle$. For the sake of simplicity, the two filter detunings are still set to be each other's opposite, i.e., $\delta_{a_1} = -\delta_{b_1} = \delta$. In Fig. 7, the second-order correlation signals $g^{(2)}(a_1, b_1)$ are presented, as a function of arbitrary delay time τ and laser detuning Δ with $\delta = 0$ in Fig. 7(a), and filter detuning δ with $\Delta = 100\gamma$ in Fig. 7(b). Other parameters are $\Omega = 100\gamma$, $\kappa = 20\gamma$. One can observe clearly from Fig. 7(a) that, for less laser detuning, for example $\Delta = 30\gamma$, the variation tendencies of antibunching for $\tau > 0$ and $\tau < 0$ are almost identical with a prominent decline for simultaneous counting. This groove in Fig. 7(a) originates from the destructive interference between two time orderings (path 6 and path 7). In detail, for $g^{(2)}(a_1, b_1, \tau > 0)$, if filter detuning is set to be zero to facilitate analysis, the emission amplitudes of positive and negative time orderings give the probability of event that photon b_1 is detected at $t + \tau$ after photon a_1 is detected at time t as $\frac{4g^2}{\kappa^2}|B_+(1 - \frac{1}{2}e^{-\frac{\kappa}{2}\tau}) - \frac{1}{2}B_-e^{-\frac{\kappa}{2}\tau}|^2$. Obviously, destructive interference occurs near $\tau = 0$, and may become incomplete for increasing filter detuning. Significantly, more instructive results emerge when Δ increase. For large laser detuning, the value of $g^{(2)}(a_1, b_1, \tau < 0)$ can be greatly suppressed, even close to zero near $\tau = 0$, but $g^{(2)}(a_1, b_1, \tau > 0)$ can remain above unity with a remarkable peak in the vicinity of simultaneous measurements. Moreover, the peak value in positive delay can be more significant with the further increase of filter detuning, as shown in Fig. 7(b).

This phenomenon can be understood as the physical distinguishability of two time orderings, leading to the definite time ordering of nonresonant cascaded emissions. As a result of sharing an initial state $|3_A\rangle$ and a final state $|1_A\rangle$, the dressed populations are irrelevant to the competition of path 6 and path 7, thus, it is just dominated by the transition amplitudes B_+ and B_-.

As mentioned in the above, for example, $\Delta = 200\gamma$ provides B_+ with larger value compared with B_-, the process of two-photon emission is mainly concentrated in path 6, as a result, if the time ordering amplitude of path 6 is selected as the positive time ordering, it dominates the detection probability of photon b_1 following the detection of a_1, i.e., $\tau > 0$. However, the amplitude of opposite time ordering

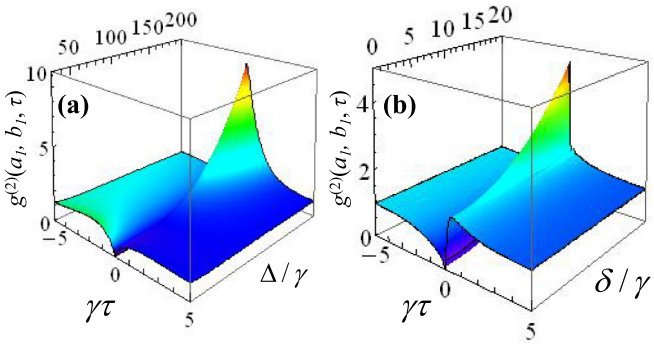

FIG. 7. Normalized second-order correlation signal $g^{(2)}(a_1, b_1, \tau)$, as a function of arbitrary delay time τ and laser detuning Δ in (a), and filter detuning δ in (b). The parameters are $\Omega = 100\gamma$, $\kappa = 20\gamma$, and $\delta = 0$ in (a), and $\Delta = 100\gamma$ in (b).

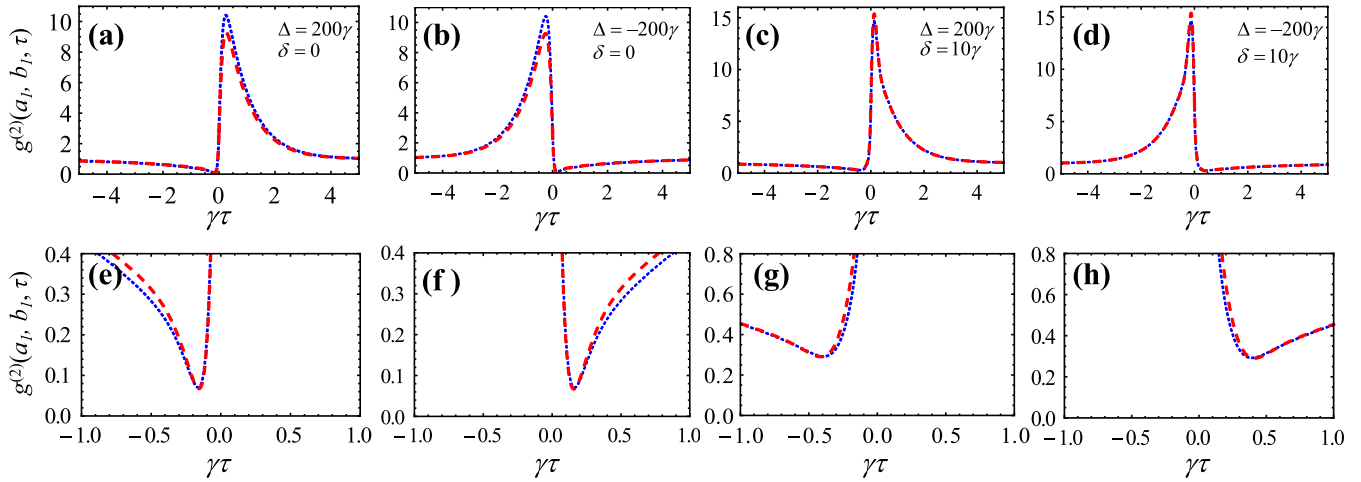

FIG. 8. Normalized second-order correlation signal $g^{(2)}(a_1, b_1, \tau)$ with $\Omega = 100\gamma$, $\kappa = 20\gamma$. The laser detuning is tuned to $\Delta = 200\gamma$ in frames (a) and (c), and $\Delta = -200\gamma$ in frames (b) and (d). The filter detuning is tuned, respectively, to $\delta = 0$ in frames (a) and (b), and $\delta = 10\gamma$ in frames (c) and (d). (e)–(h) are the enlarged views of the minimum values of (a)–(d), respectively. The red dashed thick lines and blue dashed thin lines represent the analytical results and numerical results without large width approximation, respectively.

relating to B_- only yields smaller probability with exponential decay of delay time, therefore, if the detection of photon a_1 is lagged behind the detection of photon b_1, i.e., $\tau < 0$, the result turns out to be antibunching. In addition, when the sign of laser detuning is opposite, the situations for two delays are just opposite, as illustrated in Figs. 8(a) and 8(b), or 8(c) and 8(d). This means that it is possible to effectively switch the information of emission channels with privileged time orderings through adjusting the laser frequency from red detuning to blue detuning.

In contrast, this feature can not be realized in a Mollow triplet of two-level atom, in which the nonresonant two cascaded fluorescent photons are involved to Rayleigh line and either of the sidebands. In a pair of complementary two-photon cascaded paths, not only two sideband photons are given by the same dressed state transition amplitudes, but also two Rayleigh photons (with opposite signs). This ambiguity of time orderings leads to the symmetric two-mode correlation signal.

C. Discussions and comparisons with a dressed four-level quantum dot

Apart from the two-level atom, one may naturally perceive that there is a high similarity of level structure between the three-level system under our consideration and four-level semiconductor quantum dot. The investigation of time orderings in this model was performed and many significant results were presented in Ref. [35]. Before finishing this section, let us compare our conclusions with the obtained results of four-level semiconductor quantum dot in Ref. [35].

As shown in Fig. 9(a), the bare cascaded transitions $|B\rangle \leftrightarrow |V\rangle \leftrightarrow |G\rangle$ are driven coherently by a single-mode laser field with two-photon resonance, and the fluorescent fields of interest are generated from $|B\rangle \to |H\rangle$ and $|H\rangle \to |G\rangle$ via spontaneous emissions with decay rates γ_B and γ_H, respectively. In the structure of its dressed levels in Fig. 9(b), the low-frequency fluorescent field labeled by L_0 in Ref. [35] corresponds to the transition $|1_D\rangle \to |3_D\rangle$ and is selected as one of the target spectral lines to be correlated with high-frequency spectral lines R_0 from emission $|3_D\rangle \to |1_D\rangle$ and

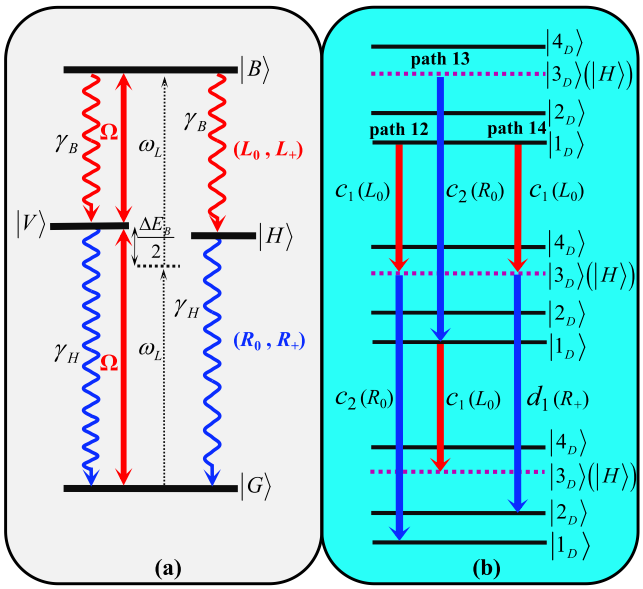

FIG. 9. (a) Level diagram for the four-level quantum dot, in which the bare transitions $|B\rangle \leftrightarrow |V\rangle \leftrightarrow |G\rangle$ are driven by a single-mode driving laser under the two-photon resonance condition $\omega_{BG} = 2\omega_L$. Two low-frequency spectral components labeled by L_0 and L_+ are radiated from $|B\rangle \to |H\rangle$ with spontaneous decay rate γ_B, and the high-frequency spectral components R_0 and R_+ are built up from $|H\rangle \to |G\rangle$ with decay rate γ_H. ΔE_B is the biexciton binding energy caused by Coulomb interactions. (b) Time orderings of fluorescent emission in dressed levels, in which the fluorescent spectral components L_0, L_+, and R_+ are equivalent to the cavity photons labeled by c_1, c_2, and d_1 respectively. The time orderings of photon pair (c_1, c_2) are depicted by path 12 and path 13, and the another isolated path 14 represents the unique time ordering of photon pair (c_1, d_1).

R_+ from emission $|3_D\rangle \to |2_D\rangle$, respectively. According to the detection theory of cavity modes, the target spectral lines L_0, R_0, and R_+ are equivalent to the cavity photons, and will be labeled by cavity mode operators c_1, c_2, and d_1 respectively in the following comparisons and discussions.

In order to probe into the physical mechanism of time orderings, the unnormalized correlations for photon pair (c_1, c_2) (i.e., the spectral lines L_0 and R_0 in Ref. [35]) in the quantum dot are derived under the conditions of large passband widths and short delay, which can be expressed compactly as

$$\begin{aligned}\mathcal{G}^{(2)}(c_1,c_2,\tau) &= \mathcal{I}_1^{(c_1)}\left|\mathcal{F}_{11}^{(c_2),+}(\tau)\right|^2 + \langle N_{33}\rangle_s\left|\mathcal{T}_{33}^{(c_1c_2),-}(\tau)\right|^2,\\ \mathcal{G}^{(2)}(c_2,c_1,\tau) &= \mathcal{I}_3^{(c_2)}\left|\mathcal{F}_{33}^{(c_1),+}(\tau)\right|^2 + \langle N_{11}\rangle_s\left|\mathcal{T}_{11}^{(c_2c_1),-}(\tau)\right|^2,\end{aligned} \tag{24}$$

with the conditional emission amplitudes

$$\begin{aligned}\mathcal{F}_{11}^{(c_2),+}(\tau) &= -ig\mu\mathcal{F}^+\left(\delta_{c_1},\delta_{c_2},\tau\right),\\ \mathcal{F}_{33}^{(c_1),+}(\tau) &= -ig\mu\mathcal{F}^+\left(\delta_{c_2},\delta_{c_1},\tau\right),\\ \mathcal{T}_{33}^{(c_1c_2),-}(\tau) &= g\mu^2\mathcal{T}^-\left(\delta_{c_1},\delta_{c_2},\tau\right),\\ \mathcal{T}_{11}^{(c_2c_1),-}(\tau) &= g\mu^2\mathcal{T}^-\left(\delta_{c_2},\delta_{c_1},\tau\right),\end{aligned} \tag{25}$$

where $\langle N_{11}\rangle_s$ and $\langle N_{33}\rangle_s$ are the steady-state populations of dressed states $|1_D\rangle$ and $|3_D\rangle$, and μ is the common dressed state transition amplitude for photons c_1 and c_2. These involving parameters are all defined in Appendix C. From Eq. (24), it is indicated that the time orderings of this photon pair are composed of two independent cascaded transition paths [path 12 and path 13 in Fig. 9(b)] with opposite emission orderings and without interference. Furthermore, two photons share a common transition amplitude, which leads to the ambiguity of two opposite time orderings. From here one may recall that the time orderings of (c_1, c_2) are the same as that of two opposite spectral sidebands of the Mollow triplet, thus, it may help us to understand the results in Ref. [35] that bunching effect is displayed from the correlated spectral lines (L_0, R_0) for positive and negative delays. By comparing the results of (a_1, a_2) and (a_1, b_2) under our consideration with this photon pair, it can be seen that although the paths of photon pairs (a_1, a_2) and (a_1, b_2) are more complicated, interference can be established. In other words, in photon pair (a_1, a_2) and (a_1, b_2), both incoherent and coherent superpositions of time orderings exist. However, the contribution of time orderings to the photon statistics of (a_1, a_2) and (a_1, b_2) are similar with the case of (c_1, c_2), because of the incoherent superposition of time orderings, the transition amplitudes can not play a great role to distinguish different time orderings.

What is more interesting is to compare the correlated photon pair (c_1, d_1) with the second group of photon pairs (a_1, b_1) in three-level system. The correlations for (c_1, d_1) are

$$\begin{aligned}\mathcal{G}^{(2)}(c_1,d_1,\tau) &= \mathcal{I}_1^{(c_1)}\left|\mathcal{F}_{12}^{(d_1),+}(\tau)\right|^2,\\ \mathcal{G}^{(2)}(d_1,c_1,\tau) &= \langle N_{11}\rangle_s\left|\mathcal{T}_{12}^{(d_1c_1),-}(\tau)\right|^2,\end{aligned} \tag{26}$$

with the conditional emission amplitudes

$$\begin{aligned}\mathcal{F}_{12}^{(d_1),+}(\tau) &= ig\frac{1}{\sqrt{2}}\mathcal{F}^+\left(\delta_{c_1},\delta_{d_1},\tau\right),\\ \mathcal{T}_{33}^{(c_1c_2),-}(\tau) &= -g\frac{\mu}{\sqrt{2}}\mathcal{T}^-\left(\delta_{d_1},\delta_{c_1},\tau\right).\end{aligned} \tag{27}$$

From these succinct forms, it is informative to note the difference of physical mechanism between (c_1, d_1) and (a_1, b_1). As depicted in Fig. 9(b), only one two-photon cascaded emission ordering is allowed for (c_1, d_1) without any other possible orderings. This isolated time ordering results in the conservation of the original time ordering in bare, as mentioned in Ref. [35]. Obviously, compared with our proposed scheme in (a_1, b_1) with a pair of complementary paths, the time ordering of (c_1, d_1) is pure and complete. This means that, for a given ordering of two-photon detection, this emission ordering is either completely positive or reverse to correlation signal, without extra paths such as those in photon pair (a_1, b_1) that the path contributing target time ordering have to be enhanced and another impedient path required to be suppressed by adjusting the pump laser detuning. This is the physical origin of bunching when the measurement of spectral line L_0 is ahead of the measurement of R_+, and antibunching for the opposite detections, i.e., the detection for L_0 is lagged behind the detection of R_+, as was shown in Ref. [35]. However, due to this conservation of time ordering in (c_1, d_1), the conversion between two different statistical properties of a photon pair under a given detection ordering may not be established, thus, although it is necessary to regulate the laser frequency for photon pair (a_1, b_1) to obtain the desired statistical property under a given detection ordering, it is this tunability and convertibility that makes the photon pairs in three-level system, such as (a_1, b_1), possess more selectivity in control of time orderings and conversion of statistical properties of photon pairs.

V. TEMPORAL INTENSITY CORRELATIONS WITH NARROW FILTER WIDTHS

So far we have systematically discussed the detection theory of FRC in the case of large filter passband widths, which provide adequate feasibility to get insight into the dressed atom-photon interactions with the help of analytical results. Finally, we supplement the case of narrow filtering $(\lambda \to 0)$ for completeness with a brief discussion.

As an example, Fig. 10(a) exhibits the second-order correlation for paired photons (a_1, a_2) in logarithmic scale varying with the detunings of two filters, in which two photons are outputted from two narrow filters with $\kappa_1 = \kappa_2 = 0.002\gamma$. We find that the statistical characteristics of filtered fluorescent

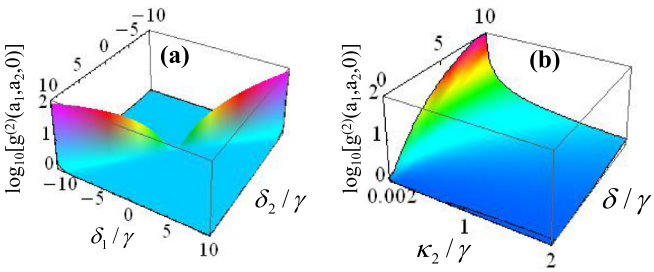

FIG. 10. Logarithmic scaled second-order correlation signals $\log_{10}[g^{(2)}(a_1, a_2, 0)]$ as functions of (δ_1, δ_2) in frame (a), and (κ_2, δ) in frame (b). The parameters are $\Omega = 100\gamma$, $\Delta = 50\gamma$, and $\kappa_1 = \kappa_2 = \kappa = 0.002\gamma$ in frame (a), and $\kappa_1 = 0.002\gamma$ with two-photon resonant condition $\delta_{a_1} = -\delta_{a_2} = \delta$ in frame (b).

photons are modified dramatically, as predicted in the Mollow triplet [38]. Except for the diagonal line of plane (δ_1, δ_2), which maintains distinct bunching, no correlation can be observed. Figure 10(b) illustrates the situation in which the linewidth of one narrow filter is fixed at $\kappa_1 = 0.002\gamma$, while the linewidth of another one is adjustable, and the detunings of two filters are opposite to each other with $\delta_1 = -\delta_2 = \delta$. In this situation, the two-mode correlation signal vanishes for larger passband, whereas it can emerge for comparable narrow linewidth of another filter, and can be enhanced by increasing filter detunings.

These statistical properties can be understood in the following physical picture. In order to select photons with high-precision setting frequency at the cost of long resolving time, i.e., $\lambda^{-1} \to \infty$, the possible emission instants that the filter can identify are distributed on the time axis taking λ^{-1} as its average resolving ability [19,44]. Therefore, whether two detectors can capture a pair of correlated photons depends on the possibility of time matching of their respective scanning ranges, which are of the order λ^{-1}. In other words, it requires the overlapping part of resolved regions on the time axis, which describes the event that the emission instant of later detected photon lies in the lifetime range of the former one, which may be realized in two filters both with narrow passbands. Therefore, two photons are generated from a common series of successive processes and bunching characteristics of two-photon cascade emission are still retained in average. Because of this requirement, it is also readily comprehensible for the case of narrow filter matched with a large passband filter yielding uncorrelated photon pairs, because there is almost no overlapping area for their lifespans on the time axis. In addition, two photons are irrelevant for extremely long delay, leading to $g^{(2)}(a_1, a_2, \tau)$ approaches to unity when $\tau \gg \lambda^{-1}$.

VI. CONCLUSION

In summary, the detection theory of FRC in filtered resonance fluorescence radiated from a Λ-type three-level atom is studied by applying the weak coupling regime between quantum emitter and cavities to probe into the interesting concept of time orderings in terms of conditional time ordering amplitudes and discussing the manipulation of time orderings. On the one hand, we are mainly interested in the limit of large filter widths and short delay region so that the mechanism of time orderings can be obviously explored through the conditioned state, which not only gives the compact analytical results of two-mode correlations, but also answers an essential question of how the filter-detector systems select time orderings——preferentially selecting positive time ordering. Meanwhile, with the help of past quantum state, the temporal two-photon correlations can be understood as the collective effect of cooperating monitoring systems. On the other hand, the features of two-mode correlation signals of three groups of photon pairs are analyzed compared with the results in the Mollow triplet and a driven four-level quantum dot. It is found that, in photon pairs with two-photon resonance, incoherent superposition of time orderings results in its indistinguishability. More interestingly, for nonresonant two-photon cascaded processes, bunching and antibunching can be obtained in two opposite detections, respectively, and the conversion of time orderings and the statistical properties of photon pair can be established in this photon pair under a given detection ordering by adjusting the pump laser frequency. This strong time asymmetry of quantum correlation originates from the fact that two different dressed state transition amplitudes of a common spectral sideband can participate in two opposite time orderings, which may be applied to complete path engineering in quantum erasure of which-path. We hope that our results could be helpful for engineering time orderings and statistical properties of resonance fluorescence in FRC.

ACKNOWLEDGMENTS

This work is supported by the National Natural Science Foundation of China (Grants No. 11774118 and No. 11474119) and the Fundamental Research Funds for the Central Universities of MOE (Grants No. CCNU18CXTD01 and No. CCNU17TS0006).

APPENDIX A: NUMERICAL METHOD OF CALCULATING CORRELATION FUNCTIONS WITHOUT LARGE FILTER WIDTH APPROXIMATION

In this Appendix, we take the photon pairs (a_1, a_2) as an example to demonstrate the numerical method of calculating second-order correlation signal $\mathcal{G}^{(2)}(a_1, a_2, \tau)$ without large filter width approximation. The other two groups of photon pairs (a_1, b_1) and (a_1, b_2) can be also treated similarly.

On the one hand, according to the quantum regression theorem [64,65], in order to calculate the delayed second-order correlation signal directly in the stationary dynamics, i.e., $\langle a_1^\dagger(t)a_2^\dagger(t+\tau)a_2(t+\tau)a_1(t)\rangle = \langle a_1^\dagger(0)(a_2^\dagger a_2)(\tau)a_1(0)\rangle$, we need the time evolution of average photon number $\langle (a_2^\dagger a_2)(\tau)\rangle$ and the initial value of correlation signal $\langle a_1^\dagger(0)a_2^\dagger(0)a_2(0)a_1(0)\rangle$. On the other hand, it serves as the steady-state solution of the equation of motion for the zero-delay correlation signal, i.e., $\frac{d}{d\tau}\langle (a_1^\dagger a_2^\dagger a_2 a_1)(\tau)\rangle$. Therefore, we start with this equation. Based on the master equation with Hamiltonian in semiclassical dressed state representation, the equation of motion for $\langle (a_1^\dagger a_2^\dagger a_2 a_1)(\tau)\rangle$, which is labeled by $\mathcal{G}$, is derived as

$$\begin{aligned}\frac{d\mathcal{G}}{d\tau} =& -(\kappa_{a_1}+\kappa_{a_2})\mathcal{G} - ig_{a_1}[B_-(u_1-u_1^*) - A_-(u_2-u_2^*)] \\ & - ig_{a_2}[A_-(u_3-u_3^*) + B_+(u_4-u_4^*)], \end{aligned} \tag{A1}$$

where the time-dependent variables $u_i (i = 1, 2, 3, 4)$ are introduced to represent the average values of the coupled operators for simplicity and clarity, i.e., we have defined $u_1 = \langle a_1^\dagger a_2^\dagger a_2 \tilde{\sigma}_{12}\rangle$, $u_2 = \langle a_1^\dagger a_2^\dagger a_2 \tilde{\sigma}_{23}\rangle$, $u_3 = \langle a_1^\dagger a_1 a_2^\dagger \tilde{\sigma}_{21}\rangle$, $u_4 = \langle a_1^\dagger a_1 a_2^\dagger \tilde{\sigma}_{32}\rangle$. Under weak coupling condition $g_i \ll \sqrt{\gamma_l \kappa_i}$, we have neglected the terms containing more cavity operators in the derivation of Eq. (A1) and the time-dependent correlation signal is coupled with the terms only one order lower than it (i.e., containing three cavity operators) through coupling constants g_{a_1} and g_{a_2}.

Obviously, the equations of motion for these introduced terms u_i containing three cavity operators are also required

to be derived, which turn out to be

$$\begin{aligned}
\frac{du_1}{d\tau} &= -\left(\frac{\kappa_{a_1}}{2}+\kappa_{a_2}+\Gamma_1-i\delta_{a_1}\right)u_1 \\
&\quad +\Gamma_4 u_2 + ig_{a_1}B_- v_1 - ig_{a_2}A_- v_2, \\
\frac{du_2}{d\tau} &= -\left(\frac{\kappa_{a_1}}{2}+\kappa_{a_2}+\Gamma_2-i\delta_{a_1}\right)u_2 \\
&\quad +\Gamma_3 u_1 + ig_{a_2}(Av_3 - B_+ v_4) - ig_{a_1}A_- v_5, \\
\frac{du_3}{d\tau} &= -\left(\frac{\kappa_{a_2}}{2}+\kappa_{a_1}+\Gamma_1-i\delta_{a_2}\right)u_3 \\
&\quad +\Gamma_4 u_4 - ig_{a_1}(Av_3{}^* + B_- v_4) + ig_{a_2}A_- v_6, \\
\frac{du_4}{d\tau} &= -\left(\frac{\kappa_{a_2}}{2}+\kappa_{a_1}+\Gamma_2-i\delta_{a_2}\right)u_4 \\
&\quad +\Gamma_3 u_3 + ig_{a_2}B_+ v_7 + ig_{a_1}A_- v_8,
\end{aligned} \tag{A2}$$

where the variables $v_i (i = 1, 2, 3, 4, 5, 6, 7, 8)$ are defined as $v_1 = \langle a_2^\dagger a_2 \tilde{\sigma}_{22}\rangle$, $v_2 = \langle a_1^\dagger a_2^\dagger \tilde{\sigma}_{11}\rangle$, $v_3 = \langle a_1^\dagger a_2 \tilde{\sigma}_{13}\rangle$, $v_4 = \langle a_1^\dagger a_2^\dagger \tilde{\sigma}_{22}\rangle$, $v_5 = \langle a_2^\dagger a_2 \tilde{\sigma}_{33}\rangle$, $v_6 = \langle a_1^\dagger a_1 \tilde{\sigma}_{11}\rangle$, $v_7 = \langle a_1^\dagger a_1 \tilde{\sigma}_{22}\rangle$, $v_8 = \langle a_1^\dagger a_2^\dagger \tilde{\sigma}_{33}\rangle$, and $v_9 = \langle a_2^\dagger a_2 \tilde{\sigma}_{11}\rangle$, $v_{10} = \langle a_1^\dagger a_1 \tilde{\sigma}_{33}\rangle$. In addition, the parameters $\Gamma_i (i = 1, 2, 3, 4)$ are of the order the atomic spontaneous decay rates. Their specific expressions are given as

$$\begin{aligned}
\Gamma_1 &= \frac{\gamma_1}{2}\Big[A_+^2 + A_-^2 + B_+^2 + B_-^2 + C_+^2 + A_+(A_+ - C_0) \\
&\quad + \frac{1}{4}(A_+ - C_0)^2\Big] \\
&\quad + \frac{\gamma_2}{2}\Big[A_+^2 + A_-^2 + B_+^2 + B_-^2 + C_-^2 + A_+(A_+ + C_0) \\
&\quad + \frac{1}{4}(A_+ + C_0)^2\Big], \\
\Gamma_2 &= \frac{\gamma_1}{2}\Big[A_+^2 + A_-^2 + B_+^2 + B_-^2 + C_-^2 + A_+(A_+ + C_0) \\
&\quad + \frac{1}{4}(A_+ + C_0)^2\Big] \\
&\quad + \frac{\gamma_2}{2}\Big[A_+^2 + A_-^2 + B_+^2 + B_-^2 + C_+^2 + A_+(A_+ - C_0) \\
&\quad + \frac{1}{4}(A_+ - C_0)^2\Big], \\
\Gamma_3 &= A_-(B_+\gamma_1 - B_-\gamma_2), \quad \Gamma_4 = A_-(B_+\gamma_2 - B_-\gamma_1),
\end{aligned} \tag{A3}$$

where the coefficients $A_\pm$, $B_\pm$, $C_\pm$, and C_0 are the dressed state transition amplitudes, which are easily obtained as $A_+ = \frac{\sin\theta\cos\theta}{\sqrt{2}}$, $A_- = \frac{\cos^2\theta}{2}$, $B_\pm = \frac{\sin\theta(1\pm\sin\theta)}{2}$, $C_\pm = \frac{\cos\theta(1\pm\sin\theta)}{2\sqrt{2}}$, and $C_0 = 2(C_+ + C_-)$. We need to point out that, in A_+ and A_-, only A_- involves the modes a_1, a_2, b_1, and b_2, therefore, the subscript "$-$" is omitted in Eq. (10) and the related equations and level diagrams, i.e., $A_- = A$. Similarly, after introducing time-dependent coupled terms with single cavity operator $w_1 = \langle a_2^\dagger \tilde{\sigma}_{32}\rangle$, $w_2 = \langle a_2^\dagger \tilde{\sigma}_{21}\rangle$, $w_3 = \langle a_1^\dagger \tilde{\sigma}_{12}\rangle$, and $w_4 = \langle a_1^\dagger \tilde{\sigma}_{23}\rangle$, the equations of motion for v_i are derived as

$$\begin{aligned}
\frac{dv_1}{d\tau} &= -\big(\kappa_{a_2}+\beta_1+\beta_2\big)v_1 \\
&\quad +\alpha_0(v_5+v_9) + ig_{a_2}A_-(w_2^* - w_2), \\
\frac{dv_2}{d\tau} &= -\left[\frac{\kappa_{a_1}+\kappa_{a_2}}{2}+\alpha_0+\alpha_1-i\big(\delta_{a_1}+\delta_{a_2}\big)\right]v_2 \\
&\quad +\beta_2 v_4 + \alpha_2 v_8 + ig_{a_1}B_- w_2, \\
\frac{dv_3}{d\tau} &= -\left[\frac{\kappa_{a_1}+\kappa_{a_2}}{2}+\beta_0-i\big(\delta_{a_1}-\delta_{a_2}\big)\right]v_3 \\
&\quad -ig_{a_2}B_+ w_3^* + ig_{a_1}B_- w_1^*, \\
\frac{dv_4}{d\tau} &= -\left[\frac{\kappa_{a_1}+\kappa_{a_2}}{2}+\beta_1+\beta_2-i\big(\delta_{a_1}+\delta_{a_2}\big)\right]v_4 \\
&\quad +\alpha_0(v_2+v_8) - ig_{a_1}A_- w_1 + ig_{a_2}A_- w_3, \\
\frac{dv_5}{d\tau} &= -\big(\kappa_{a_2}+\alpha_0+\alpha_2\big)v_5 \\
&\quad +\alpha_1 v_9 + \beta_1 v_1 + ig_{a_2}B_+(w_1^* - w_1), \\
\frac{dv_6}{d\tau} &= -\big(\kappa_{a_1}+\alpha_0+\alpha_1\big)v_6 \\
&\quad +\alpha_2 v_{10} + \beta_2 v_7 + ig_{a_1}B_-(w_3^* - w_3), \\
\frac{dv_7}{d\tau} &= -\big(\kappa_{a_1}+\beta_1+\beta_2\big)v_7 \\
&\quad +\alpha_0(v_6+v_{10}) - ig_{a_1}A_-(w_4^* - w_4), \\
\frac{dv_8}{d\tau} &= -\left[\frac{\kappa_{a_1}+\kappa_{a_2}}{2}+\alpha_0+\alpha_2-i\big(\delta_{a_1}+\delta_{a_2}\big)\right]v_8 \\
&\quad +\beta_1 v_4 + \alpha_1 v_2 + ig_{a_2}B_+ w_4, \\
\frac{dv_9}{d\tau} &= -\big(\kappa_{a_2}+\alpha_0+\alpha_1\big)v_9 + \alpha_2 v_5 + \beta_2 v_1, \\
\frac{dv_{10}}{d\tau} &= -\big(\kappa_{a_1}+\alpha_0+\alpha_2\big)v_{10} + \alpha_1 v_6 + \beta_1 v_7,
\end{aligned} \tag{A4}$$

with the parameters being the same order as atomic spontaneous decay rates

$$\begin{aligned}
&\alpha_0 = A_-^2(\gamma_1+\gamma_2), \quad \alpha_1 = C_+^2\gamma_1 + C_-^2\gamma_2, \\
&\alpha_2 = C_+^2\gamma_2 + C_-^2\gamma_1, \\
&\beta_0 = \tfrac{1}{2}(\gamma_1+\gamma_2)\big(2A_-^2 + C_0^2 + C_+^2 + C_-^2\big), \\
&\beta_1 = B_+^2\gamma_1 + B_-^2\gamma_2, \quad \beta_2 = B_+^2\gamma_2 + B_-^2\gamma_1.
\end{aligned} \tag{A5}$$

The newly introduced time-dependent coupled terms w_1, w_2, w_3, and w_4 are only coupled with the dressed populations

$$\begin{aligned}
\frac{dw_1}{d\tau} &= -\left(\frac{\kappa_{a_2}}{2}+\Gamma_2-i\delta_{a_2}\right)w_1 + ig_{a_2}B_+\langle\tilde{\sigma}_{22}\rangle + \Gamma_3 w_2, \\
\frac{dw_2}{d\tau} &= -\left(\frac{\kappa_{a_2}}{2}+\Gamma_1-i\delta_{a_2}\right)w_2 + ig_{a_2}A_-\langle\tilde{\sigma}_{11}\rangle + \Gamma_4 w_1, \\
\frac{dw_3}{d\tau} &= -\left(\frac{\kappa_{a_1}}{2}+\Gamma_1-i\delta_{a_1}\right)w_3 + ig_{a_1}B_-\langle\tilde{\sigma}_{22}\rangle + \Gamma_4 w_4, \\
\frac{dw_4}{d\tau} &= -\left(\frac{\kappa_{a_1}}{2}+\Gamma_2-i\delta_{a_1}\right)w_4 - ig_{a_1}A_-\langle\tilde{\sigma}_{33}\rangle + \Gamma_3 w_3.
\end{aligned} \tag{A6}$$

It can be noticed that, in addition to the equation of motion for correlation signal in Eq. (A1), all of the above equations contain linear terms about atomic spontaneous emission rates, Γ_1, Γ_2, Γ_3, Γ_4, α_0, α_1, α_2, β_0, β_1, and β_2, making it difficult to obtain the steady-state solutions analytically. Therefore, when these items are taken into consideration, the correlation function is obtained numerically, which gives the blue dashed thin lines in Figs. 5(c), 5(d) and Figs. 8(a)–8(h) in Sec. IV.

However, fortunately, under the condition of large filter widths, all the terms involving atomic spontaneous emission rates in the above equations can be neglected, therefore, the steady-state solution of each coupled equation can be solved analytically and gives the analytical results of the correlations.

APPENDIX B: DERIVATION OF TWO-MODE CORRELATIONS FOR ARBITRARY TIME DELAY WITH LARGE FILTER WIDTHS

Following the obtained coupled equations of motion, we still take the photon pairs (a_1, a_2) as an example to derive the unnormalized second-order correlation $\mathcal{G}^{(2)}(a_1, a_2, \tau)$ for arbitrary detection time difference in the limit of large passband widths. Another two results $\mathcal{G}^{(2)}(a_1, b_1, \tau)$ and $\mathcal{G}^{(2)}(a_1, b_2, \tau)$ can be also obtained straightforwardly.

For arbitrary delay, the unnormalized correlation function should be directly calculated from the superposition of probability components $\langle a_1^\dagger a_1 (a_2^\dagger a_2 \tilde{\sigma}_{11})(\tau)\rangle$, $\langle a_1^\dagger a_1 (a_2^\dagger a_2 \tilde{\sigma}_{22})(\tau)\rangle$, and $\langle a_1^\dagger a_1 (a_2^\dagger a_2 \tilde{\sigma}_{33})(\tau)\rangle$, labeled by $\mathcal{G}_1$, $\mathcal{G}_2$, and $\mathcal{G}_3$, respectively. According to the quantum regression theorem, the time evolutions of $\mathcal{G}_1$, $\mathcal{G}_2$, and $\mathcal{G}_3$ are dominated by the equations of motion for v_1, v_5, and v_9 in Appendix A with the help of large passband widths approximation

$$\begin{aligned}
\frac{dv_9}{d\tau} &\approx -\kappa_{a_2} v_9, \\
\frac{dv_1}{d\tau} &\approx -\kappa_{a_2} v_1 + i g_{a_2} A (w_2^* - w_2), \\
\frac{dv_5}{d\tau} &\approx -\kappa_{a_2} v_5 + i g_{a_2} B_+ (w_1^* - w_1),
\end{aligned} \tag{B1}$$

where the time-dependent coupling terms w_1 and w_2 are governed by their equations of motion

$$\begin{aligned}
\frac{dw_1}{d\tau} &\approx -\left(\frac{\kappa_{a_2}}{2} - i\delta_{a_2}\right) w_1 + i g_{a_2} B_+ \langle \tilde{\sigma}_{22}\rangle, \\
\frac{dw_2}{d\tau} &\approx -\left(\frac{\kappa_{a_2}}{2} - i\delta_{a_2}\right) w_2 + i g_{a_2} A \langle \tilde{\sigma}_{11}\rangle.
\end{aligned} \tag{B2}$$

Meanwhile, after applying quantum regression theorem to Eq. (B1) to obtain the equations of motion for $\mathcal{G}_1$, $\mathcal{G}_2$, and $\mathcal{G}_3$, its steady-state values, $\mathcal{G}_{1s}$, $\mathcal{G}_{2s}$, and $\mathcal{G}_{3s}$, are solved to be the initial values of time-dependent probability components, which are derived straightforwardly as

$$\begin{aligned}
\mathcal{G}_{1s} &= \frac{i g_{a_1} B_- (u_{1s}^* - u_{1s})}{\kappa_{a_1} + \kappa_{a_2}}, \quad \mathcal{G}_{3s} = \frac{i g_{a_2} B_+ (u_{4s}^* - u_{4s})}{\kappa_{a_1} + \kappa_{a_2}}, \\
\mathcal{G}_{2s} &= \frac{i g_{a_1} A (u_{2s} - u_{2s}^*)}{\kappa_{a_1} + \kappa_{a_2}} - \frac{i g_{a_2} A (u_{3s} - u_{3s}^*)}{\kappa_{a_1} + \kappa_{a_2}}.
\end{aligned} \tag{B3}$$

The steady-state values of coupling terms in Eq. (B3) can also be obtained iteratively from the corresponding equations of motion in Appendix A. With these steady-state solutions in hand and after some algebraic arrangements, the total unnormalized second-order correlation function of photon pairs (a_1, a_2) for arbitrary delay can be divided into two parts

$$\mathcal{G}^{(2)}(a_1, a_2, \tau) = \mathcal{G}_{sd}^{(2)}(a_1, a_2, \tau) + \mathcal{G}_{ld}^{(2)}(a_1, a_2, \tau). \tag{B4}$$

The first term is the short delay behavior given by Eq. (16) and labeled as $\mathcal{G}_{sd}^{(2)}(a_1, a_2, \tau)$ in Eq. (B4). The second part takes the form of

$$\mathcal{G}_{ld}^{(2)}(a_1, a_2, \tau) = \frac{\eta_1 (e^{-r_1\tau} - 1) + \eta_2 (e^{-r_2\tau} - 1)}{\left[\left(\frac{\kappa_{a_1}}{2}\right)^2 + \delta_{a_1}^2\right]\left[\left(\frac{\kappa_{a_2}}{2}\right)^2 + \delta_{a_2}^2\right]}, \tag{B5}$$

which comes from the consideration of long delay behavior. Its time evolution is only determined by the parameters, η_1, η_2, r_1, r_2, of the dressed atom. The parameters η_1, η_2 are defined as

$$\eta_1 = \frac{\xi_{12}\langle\tilde{\sigma}_{22}\rangle_s + \xi_{13}\langle\tilde{\sigma}_{33}\rangle_s}{r_1(r_2 - r_1)}, \quad \eta_2 = \frac{\xi_{22}\langle\tilde{\sigma}_{22}\rangle_s + \xi_{23}\langle\tilde{\sigma}_{33}\rangle_s}{r_2(r_1 - r_2)}, \tag{B6}$$

in which ξ_{12}, ξ_{13}, ξ_{22}, and ξ_{23} are given by

$$\begin{aligned}
\xi_{12} &= A^2 B_-^2 \left[-r_1^2 + r_1(\mathcal{R}_1 + \mathcal{R}_{31}) - \mathcal{S}_2\right] \\
&\quad + B_+^2 B_-^2 (r_1 \mathcal{R}_{12} - \mathcal{S}_3), \\
\xi_{13} &= A^2 B_+^2 \left[-r_1^2 + r_1(\mathcal{R}_2 + \mathcal{R}_{32}) - \mathcal{S}_3\right] \\
&\quad + A^4 (r_1 \mathcal{R}_{21} - \mathcal{S}_2), \\
\xi_{22} &= A^2 B_-^2 \left[-r_2^2 + r_2(\mathcal{R}_1 + \mathcal{R}_{31}) - \mathcal{S}_2\right] \\
&\quad + B_+^2 B_-^2 (r_2 \mathcal{R}_{12} - \mathcal{S}_3), \\
\xi_{23} &= A^2 B_+^2 \left[-r_2^2 + r_2(\mathcal{R}_2 + \mathcal{R}_{32}) - \mathcal{S}_3\right] \\
&\quad + A^4 (r_2 \mathcal{R}_{21} - \mathcal{S}_2),
\end{aligned} \tag{B7}$$

where the coefficients relating to the dressed transition rates $\mathcal{R}_{ij}$ are defined as

$$\begin{aligned}
\mathcal{R}_1 &= \mathcal{R}_{21} + \mathcal{R}_{23} + \mathcal{R}_{32}, \\
\mathcal{R}_2 &= \mathcal{R}_{12} + \mathcal{R}_{13} + \mathcal{R}_{31}, \\
\mathcal{R}_3 &= \mathcal{R}_{21} - \mathcal{R}_{31}, \quad \mathcal{R}_4 = \mathcal{R}_{12} - \mathcal{R}_{32}, \\
\mathcal{S}_1 &= (\mathcal{R}_{21} - \mathcal{R}_{31})(\mathcal{R}_{12} - \mathcal{R}_{32}), \\
\mathcal{S}_2 &= \mathcal{R}_{32}\mathcal{R}_3 + \mathcal{R}_{31}\mathcal{R}_1, \\
\mathcal{S}_3 &= \mathcal{R}_{31}\mathcal{R}_4 + \mathcal{R}_{32}\mathcal{R}_2,
\end{aligned} \tag{B8}$$

with $2r_{1,2} = (\mathcal{R}_1 + \mathcal{R}_2) \mp \sqrt{(\mathcal{R}_1 - \mathcal{R}_2)^2 + 4\mathcal{R}_3}$, and the transition rates can be easily found. Therefore, we obtain the unnormalized correlation function for arbitrary time difference given by Eq. (16) with Eq. (B5). It is easy to verify that the uncorrelated condition of normalized correlation function $g^{(2)}(a_1, a_2, \tau) = \mathcal{G}^{(2)}(a_1, a_2, \tau)/\langle a_1^\dagger a_1\rangle_s \langle a_2^\dagger a_2\rangle_s$ is satisfied, i.e., $\lim_{\tau\to\infty} g^{(2)}(a_1, a_2, \tau) = 1$. In addition, we would like to examine the behaviors of $\mathcal{G}^{(2)}(a_1, a_2, \tau)$ in the limit of long delay time and infinite bandwidths (color-blind filters). Because of $\kappa \gg \gamma$, all the exponential decays depending on κ disappear, and only those depended on the parameters r_1 and r_2, which are of the order γ, can survive. Then, the

unnormalized correlation function is simplified as

$$\lim_{\kappa\gg\gamma}\mathcal{G}^{(2)}(a_1,a_2,\tau)=\frac{\mathcal{G}_0^{(2)}(a_1,a_2,\tau)}{\left[\left(\frac{\kappa_{a_1}}{2}\right)^2+\delta_{a_1}^2\right]\left[\left(\frac{\kappa_{a_2}}{2}\right)^2+\delta_{a_2}^2\right]}, \tag{B9}$$

with numerator

$$\begin{aligned}\mathcal{G}_0^{(2)}(a_1,a_2,\tau)=&A^2B_-^2\langle\tilde{\sigma}_{22}\rangle_s\mathcal{P}_{1\to1}(\tau)+A^4\langle\tilde{\sigma}_{33}\rangle_s\mathcal{P}_{2\to1}(\tau)\\&+B_+^2B_-^2\langle\tilde{\sigma}_{22}\rangle_s\mathcal{P}_{1\to2}(\tau)\\&+A_+^2B_+^2\langle\tilde{\sigma}_{33}\rangle_s\mathcal{P}_{2\to2}(\tau),\end{aligned} \tag{B10}$$

where $\mathcal{P}_{k\to k'}(\tau)=|\langle k_A(0)|k'_A(\tau)\rangle|^2$ stands for the evolution probability of the dressed atom from the final dressed state $|k_A\rangle$ of the transition responsible for emitting a photon a_1 to the dressed state $|k'_A\rangle$ being the initial state of the next transition for emitting photon a_2. This indicates that the correlation function in Eq. (B10) describes the simple dynamics of free evolution of the dressed atom with spontaneous decays. Therefore, in the limit of long delay, unnormalized correlation function in Eq. (B9) is essentially the standard correlation function, which is just modulated by the Lorentzian filter response functions. After normalization, $g^{(2)}(a_1,a_2,\tau)$ is independent of the information of filters, and returns to the standard form, i.e., $g^{(2)}(a_1,a_2,\tau)=g_0^{(2)}(a_1,a_2,\tau)$ for $\tau\gg\lambda^{-1}$. Similarly, for infinite bandwidth, the parameters of filters also vanish for color-blind filters and the physical requirement $\lim_{\lambda\to\infty}g^{(2)}(a_1,a_2,\tau)=g_0^{(2)}(a_1,a_2,\tau)$ is still conserved.

APPENDIX C: DRESSED STATES AND CORRELATIONS FOR ARBITRARY DELAY OF THE FOUR-LEVEL QUANTUM DOT

In this Appendix, we present the dressed states of the quantum dot modeled by a four-level system to determine the correlated target spectral bands in Ref. [35], and then, being an example, the correlation function of photon pair (c_1,c_2) for arbitrary delay is given in brief.

The Hamiltonian of the driven four-level quantum dot is

$$\begin{aligned}H_{QD}=&\hbar\Delta_B\sigma_{BB}+\hbar\Delta_V\sigma_{VV}+\hbar\Delta_H\sigma_{HH}\\&+\Omega_G(\sigma_{GV}+\sigma_{VG})+\Omega_B(\sigma_{BV}+\sigma_{VB}),\end{aligned} \tag{C1}$$

where the different laser detunings are defined as $\Delta_V=\omega_{VG}-\omega_L$, $\Delta_H=\omega_{HG}-\omega_L$, and $\Delta_B=\omega_{BG}-2\omega_L$. For the sake of simplicity, the condition of two-photon resonance is assumed to be satisfied, i.e., $\Delta_B=0$. Meanwhile, two Rabi frequencies (Ω_B,Ω_G) and two detunings (Δ_V,Δ_H) are both set to be equal, i.e., $\Omega_B=\Omega_G=\Omega$ and $\Delta_V=\Delta_H=\Delta E_B/2=\Delta$ (ΔE_B is biexciton binding energy caused by Coulomb interactions). After diagonalization of H_{QD}, we obtain the semiclassical dressed eigenstates $|1_D\rangle$, $|2_D\rangle$, $|3_D\rangle$, and $|4_D\rangle$ that are expressed in term of the bare states as

$$\begin{pmatrix}|4_D\rangle\\|3_D\rangle\\|2_D\rangle\\|1_D\rangle\end{pmatrix}=\begin{pmatrix}\epsilon_1&\epsilon_2&0&\epsilon_1\\0&0&1&0\\\frac{1}{\sqrt{2}}&0&0&-\frac{1}{\sqrt{2}}\\\epsilon_3&\epsilon_4&0&\epsilon_3\end{pmatrix}\begin{pmatrix}|B\rangle\\|V\rangle\\|H\rangle\\|G\rangle\end{pmatrix}, \tag{C2}$$

where the parameters are defined as

$$\epsilon_{1,3}=\frac{1}{\sqrt{2+\left(\frac{\Delta\pm\Omega_0}{2\Omega}\right)^2}},\quad \epsilon_{2,4}=\frac{1}{2\Omega}\frac{\Delta\pm\Omega_0}{\sqrt{2+\left(\frac{\Delta\pm\Omega_0}{2\Omega}\right)^2}} \tag{C3}$$

with $\Omega_0=\sqrt{\Delta^2+8\Omega^2}$. With these in hand, the bare emission operators of interest can be decomposed into

$$\begin{aligned}\sigma_{HB}&=\sigma_{L_0}^-+\sigma_{L_+}^-+\sigma_{R_1}^-\\&=(\mu_2N_{31})+\left(\frac{1}{\sqrt{2}}N_{32}\right)+(\mu_4N_{34}),\\\sigma_{GH}&=\sigma_{R_0}^-+\sigma_{R_+}^-+\sigma_{L_1}^-\\&=(\mu_2N_{13})+\left(\frac{-1}{\sqrt{2}}N_{23}\right)+(\mu_4N_{43}),\end{aligned} \tag{C4}$$

with the transition amplitudes

$$\mu_{1,3}=\pm\frac{\epsilon_{1,3}}{2(\epsilon_1\epsilon_4-\epsilon_2\epsilon_3)},\quad \mu_{2,4}=\mp\frac{\epsilon_{1,2}}{2(\epsilon_1\epsilon_4-\epsilon_2\epsilon_3)}. \tag{C5}$$

Where $N_{kk'}$ are the emission operators of dressed quantum dot from the dressed state $|k'_D\rangle$ to $|k_D\rangle$, i.e., $N_{kk'}=|k_D\rangle\langle k'_D|$. Apparently, in the emission spectrum, the bare low-frequency radiation $|B\rangle\to|H\rangle$ contributes two low-frequency fluorescent bands L_0, L_+ and one high-frequency band R_1, and the bare high-frequency radiation $|H\rangle\to|G\rangle$ generates two high-frequency fluorescent bands R_0, R_+ and one low-frequency band L_1. More coincidentally, the fluorescent photons L_0 and R_0 share a common dressed state transition amplitude μ_2 [labeled by μ in Eqs. (25) and (27)]. With these operators, the target spectral components L_0, R_0 and R_+ can be correlated, which are given in Eqs. (24) and (26).

Taking the photon pair (c_1,c_2) as an example, the unnormalized correlation function for arbitrary time delay can also be decomposed into two parts as

$$\mathcal{G}^{(2)}(c_1,c_2,\tau)=\mathcal{G}_{sd}^{(2)}(c_1,c_2,\tau)+\mathcal{G}_{ld}^{(2)}(c_1,c_2,\tau), \tag{C6}$$

where the first term represents its short-time behavior given by Eq. (24), and the second term

$$\mathcal{G}_{ld}^{(2)}(c_1,c_2,\tau)=\frac{\mathcal{G}_0^{(2)}(c_1,c_2,\tau)-\mu_2^4\langle N_{11}\rangle_s}{\left[\left(\frac{\kappa}{2}\right)^2+\delta_{c_1}^2\right]\left[\left(\frac{\kappa}{2}\right)^2+\delta_{c_2}^2\right]} \tag{C7}$$

is the correction term when the long-time behavior is taken into account. This form ensures the automatic degradation of correlation signal from the filtered form to the standard form under the condition of long delay (modulated by two Lorentzian spectral functions, which will vanish algebraically after normalization), which has been demonstrated in Appendix B. The steady-state dressed populations $\langle N_{11}\rangle_s$ can be easily obtained from its equations of motion, which takes the form of rate equations.

[1] D. F. Walls and G. J. Milburn, *Quantum Optics* (Springer, Berlin, 2008).

[2] A. Aspect, P. Grangier, and G. Roger, Phys. Rev. Lett. **49**, 91 (1982).

[3] T. Yamamoto, M. Koashi, S. K. Ozdemir, and N. Imoto, Nature (London) **421**, 343 (2003).

[4] A. C. Dada, J. Leach, G. S. Buller, M. J. Padgett, and E. Andersson, Nat. Phys. **7**, 677 (2011).

[5] A. K. Ekert, Phys. Rev. Lett. **67**, 661 (1991).

[6] H.-J. Briegel, W. Dür, J. I. Cirac, and P. Zoller, Phys. Rev. Lett. **81**, 5932 (1998).

[7] J.-C. Boileau, R. Laflamme, M. Laforest, and C. R. Myers, Phys. Rev. Lett. **93**, 220501 (2004).

[8] A. Vaziri, G. Weihs, and A. Zeilinger, Phys. Rev. Lett. **89**, 240401 (2002).

[9] A. Dousse, J. Suffczyński, A. Beveratos, O. Krebs, A. Lemaître, I. Sagnes, J. Bloch, P. Voisin, and P. Senellart, Nature (London) **466**, 217 (2010).

[10] A. González-Tudela, E. del Valle, and F. P. Laussy, Phys. Rev. A **91**, 043807 (2015).

[11] C. Sánchez Muñoz, E. del Valle, C. Tejedor, and F. P. Laussy, Phys. Rev. A **90**, 052111 (2014).

[12] M. Peiris, B. Petrak, K. Konthasinghe, Y. Yu, Z. C. Niu, and A. Muller, Phys. Rev. B **91**, 195125 (2015).

[13] M. Peiris, K. Konthasinghe, and A. Muller, Phys. Rev. Lett. **118**, 030501 (2017).

[14] A. Ulhaq, S. Weiler, S. M. Ulrich, R. Roßbach, M. Jetter, and P. Michler, Nat. Photon. **6**, 238 (2012).

[15] F. P. Laussy, Nat. Mater. **16**, 398 (2017).

[16] G. Bel and F. L. H. Brown, Phys. Rev. Lett. **102**, 018303 (2009).

[17] S. L. Portalupi, M. Widmann, C. Nawrath, M. Jetter, P. Michler, J. Wrachtrup, and I. Gerhardt, Nat. Commun. **7**, 13632 (2016).

[18] Y. Ben-Aryeh, H. Freedhoff, and T. Rudolph, J. Opt. B. **1**, 624 (1999).

[19] A. Gonzalez-Tudela, F. P. Laussy, C. Tejedor, M. J. Hartmann, and E. del Valle, New J. Phys. **15**, 033036 (2013).

[20] J. C. L. Carreño, E. del Valle, and F. P. Laussy, Laser Photon. Rev. **11**, 1700090 (2017).

[21] T. H. Chung, G. Juska, S. T. Moroni, A. Pescaglini, A. Gocalinska, and E. Pelucchi, Nat. Photon. **10**, 782 (2016).

[22] H. Jayakumar, A. Predojević, T. Kauten, T. Huber, G. Solomon, and G. Weihs, Nat. Commun. **5**, 4251 (2014).

[23] Y. M. He, O. Iff, N. Lundt, V. Baumann, M. Davanco, K. Srinivasan, S. Höfling, and C. Schneider, Nat. Commun. **7**, 13409 (2016).

[24] K. D. Jöns, L. Schweickert, M. A. M. Versteegh, D. Dalacu, P. J. Poole, A. Gulinatti, A. Giudice, V. Zwiller, and M. E. Reimer, Sci. Rep. **7**, 1700 (2017).

[25] N. Akopian, N. H. Lindner, E. Poem, Y. Berlatzky, J. Avron, D. Gershoni, B. D. Gerardot, and P. M. Petroff, Phys. Rev. Lett. **96**, 130501 (2006).

[26] A. Muller, W. Fang, J. Lawall, and G. S. Solomon, Phys. Rev. Lett. **103**, 217402 (2009).

[27] R. J. Young, R. M. Stevenson, P. Atkinson, K. Cooper, D. A. Ritchie, and A. J. Shields, New J. Phys. **8**, 29 (2006).

[28] E. del Valle, New J. Phys. **15**, 025019 (2013).

[29] R. Hafenbrak, S. M. Ulrich, P. Michler, L. Wang, A. Rastelli, and O. G. Schmidt, New J. Phys. **9**, 315 (2007).

[30] Y. N. Sun, Y. Zou, G. Chen, J. S. Tang, H. Q. Ni, M. F. Li, G. W. Zha, Z. C. Niu, Y. J. Han, C. F. Li, and G. C. Guo, Opt. Express **25**, 1778 (2017).

[31] E. Moreau, I. Robert, L. Manin, V. Thierry-Mieg, J. M. Gérard, and I. Abram, Phys. Rev. Lett. **87**, 183601 (2001).

[32] A. Kiraz, S. Fälth, C. Becher, B. Gayral, W. V. Schoenfeld, P. M. Petroff, L. Zhang, E. Hu, and A. Imamoglu, Phys. Rev. B **65**, 161303(R) (2002).

[33] C. A. Schrama, G. Nienhuis, H. A. Dijkerman, C. Steijsiger, and H. G. M. Heideman, Phys. Rev. A **45**, 8045 (1992).

[34] G. Nienhuis, Phys. Rev. A **47**, 510 (1993).

[35] S. Bounouar, M. Strauß, A. Carmele, P. Schnauber, A. Thoma, M. Gschrey, J.-H. Schulze, A. Strittmatter, S. Rodt, A. Knorr, and S. Reitzenstein, Phys. Rev. Lett. **118**, 233601 (2017).

[36] C. A. Schrama, G. Nienhuis, H. A. Dijkerman, C. Steijsiger, and H. G. M. Heideman, Phys. Rev. Lett. **67**, 2443 (1991).

[37] H. F. Arnoldus and G. Nienhuis, J. Phys. B **17**, 963 (1984).

[38] G. Nienhuis, Europhys. Lett. **21**, 285 (1993).

[39] P. Zhou and S. Swain, Phys. Rev. A **58**, 1515 (1998).

[40] J. E. Avron, G. Bisker, D. Gershoni, N. H. Lindner, E. A. Meirom, and R. J. Warburton, Phys. Rev. Lett. **100**, 120501 (2008).

[41] E. del Valle, A. Gonzalez-Tudela, F. P. Laussy, C. Tejedor, and M. J. Hartmann, Phys. Rev. Lett. **109**, 183601 (2012).

[42] K. Kamide, S. Iwamoto, and Y. Arakawa, Phys. Rev. A **92**, 033833 (2015).

[43] V. N. Shatokhin and S. Y. Kilin, Phys. Rev. A **94**, 033835 (2016).

[44] K. Joosten and G. Nienhuis, J. Opt. B. **2**, 158 (2000).

[45] C. Cohen-Tannoudji and S. Reynaud, Philos. Trans. R. Soc. Lond. A **293**, 223 (1979).

[46] V. N. Shatokhin and S. Y. Kilin, Phys. Rev. A **63**, 023803 (2001).

[47] V. N. Shatokhin and S. Y. Kilin, Opt. Commun. **174**, 157 (2000).

[48] V. N. Shatokhin and S. Y. Kilin, Opt. Commun. **210**, 291 (2002).

[49] S. Gammelmark, B. Julsgaard, and K. Molmer, Phys. Rev. Lett. **111**, 160401 (2013).

[50] L. Knöll, G. Weber, and T. Schäfer, J. Phys. B **17**, 4861 (1984).

[51] J. Wiersig, C. Gies, F. Jahnke, M. Aßmann, T. Berstermann, M. Bayer, C. Kistner, S. Reitzenstein, C. Schneider, S. Höfling, A. Forchel, C. Kruse, J. Kalden, and D. Hommel, Nature (London) **460**, 245 (2009).

[52] J. Dalibard and S. Reynaud, J. Phys. (Paris) **44**, 1337 (1983).

[53] L. Knöll and G. Weber, J. Phys. B **19**, 2817 (1986).

[54] L. Knöll, W. Vogel, and D.-G. Welsch, Phys. Rev. A **42**, 503 (1990).

[55] J. H. Eberly and K. Wodkiewicz, J. Opt. Soc. Am. **67**, 1252 (1977).

[56] J. D. Cresser, J. Phys. B **20**, 4915 (1987).

[57] M. O. Scully and M. S. Zubairy, *Quantum Optics* (Cambridge University Press, Cambridge, 1997).

[58] C. Cohen-Tannoudji, J. Dupont-Roc, and G. Grynberg, *Atom-Photon Interactions* (Wiley, New York, 1992).

[59] B. M. Garraway, Phys. Rev. A **55**, 2290 (1997).
[60] J. S. Peng and G. X. Li, *Introduction to Modern Quantum Optics* (World Scientific, Singapore, 1998).
[61] P. Campagne-Ibarcq, L. Bretheau, E. Flurin, A. Auffèves, F. Mallet, and B. Huard, Phys. Rev. Lett. **112**, 180402 (2014).
[62] D. Tan, N. Foroozani, M. Naghiloo, A. H. Kiilerich, K. Molmer, and K. W. Murch, Phys. Rev. A **96**, 022104 (2017).
[63] Q. Xu and K. Molmer, Phys. Rev. A **92**, 033830 (2015).
[64] M. Lax, Phys. Rev. **129**, 2342 (1963).
[65] P. Meystre and M. Sargent, *Elements of Quantum Optics* (Springer, Berlin, 2007).